LIÈGE université
Gembloux
Agro-Bio Tech

Monitoring vegetation seasonality in Central Africa using Sentinel-2 data

Léna Royen

Travail de fin d'étude présenté en vue de l'obtention du diplôme de master bioingénieur
Sciences et Technologies de l'Environnement

Année académique 2020-2021

Co-promoteurs: Pr. Adeline Fayolle (Uliège) & Dr. Jean-Baptiste Féret (INRAE)

[1] In this case, the academic authority is represented by the promoter(s) member(s) of the teaching staff of GxABT

[2] Dans ce cas, l'autorité académique est représentée par le(s) promoteur(s) membre(s) du personnel enseignant de GxABT

LIÈGE université
Gembloux
Agro-Bio Tech

Monitoring vegetation seasonality in Central Africa using Sentinel-2 data

Léna Royen

Travail de fin d'étude présenté en vue de l'obtention du diplôme de master bioingénieur
Sciences et Technologies de l'Environnement

Année académique 2020-2021

Co-promoteurs: Pr. Adeline Fayolle (Uliège) & Dr. Jean-Baptiste Féret (INRAE)

This master thesis was carried out in partnership with the French National Research Institute for Agriculture, Food and the Environment (INRAE) in the premises of the "Maison de la télédétection" in Montpellier and of Gembloux Agro-Bio Tech.

The University of Liege and the Erasmus programme provided financial support to the author under a mobility contract for a student placement in the European Union.

Acknowledgements

I would like to express my special thanks of gratitude to those who, from near or far, have participated in this work.

Firstly, I am grateful to Adeline Fayolle who was an incredible promotor that helped me to get confidence in my abilities. I also would like to deeply thank Jean-Baptiste Féret and his institution, the National Research Institute for Agriculture, Food and the Environment (INRAE) who welcomed me warmly.

I am very thankful to the tropical forestry team, for your precious time and advice. A particular thanks to Anais-Phasiphaé Gorel for the proofreading and pertinent remarks. I am also very thankful to Jonathan Bitton for his availability and listening skills.

Furthermore, I would like to mention the fieldworkers that acquired the ground data necessary for my work.

I would like to extend my heartfelt thanks to my mum and dad for their unconditional love and encouragement. To my brother, Jonas, our friendship and mutual support are precious to me. To my sisters Annie and Elise who always covered my back. A special thanks to Johan, my beloved secretary, who dared to endure my stress during this period.

At last, thank you, Thomas, Marie, Tanguy and Daphné, you embellished these five years of study. I finally would like to thank my long-time friends, Romane and Julia, you gave me so much support.

Abstract

Tropical forests in Central Africa are found under dry and seasonal climates. The vegetation adopts a seasonal pattern as depicted by localized field studies, but its importance and extent are barely known. The recent Sentinel-2 mission provides new opportunities to monitor vegetation phenology from space.

The first objective of this study was to assess the potential of Sentinel-2 data to monitor vegetation seasonality in Central Africa. The use of Sentinel-2 data further aimed to address the questions of how seasonal are Central African forests, and how is this seasonal functioning related to rainfall seasonality in Central African Republic (Mbaïki) and Democratic Republic of Congo (Luki) subjected to reverse rainfall regimes. This work relied on three data types: (i) Sentinel-2 images, (ii) ground data consisting of regular observations of phenophases and (iii) rainfall data from the Global Precipitation Measurement mission.

The resulting rainfall and Enhanced Vegetation Index times series allowed respectively the retrieval of the start of rain and the start of the season further compared to the ground observations. An additional wavelet analysis was performed on the Mbaïki site to determine the frequency and timing of the periodic vegetation events.

This work has demonstrated the suitability of the recently available Sentinel-2 data for monitoring vegetation dynamics when cloud contamination remains reasonable. In addition, annual vegetation cycles dominated at the study sites, in line with the seasonality of rainfall. Comparison between sites confirmed a shift in vegetation seasonality from Mbaïki to Luki in response to the inversion of rainfall patterns across the Equator. In Mbaïki, the forest EVI signal was on average 16.9 $\pm$ 4.4 days before the rainfall signal, supporting the ultimate control of rainfall. In contrast, for both study sites, the earliest onset of rainfall resulted in the earliest onset of the season in 2019, supporting the hypothesis that rainfall exert a proximal control.

To conclude, Sentinel-2 data are suited to monitor vegetation seasonality but would require the combination with additional images to cope with continuously clouded areas.

Keywords: Remote sensing, Phenology, Sentinel-2, Tropical forests, Central Africa, Enhanced Vegetation Index.

Résumé

Les forêts tropicales d'Afrique centrale se trouvent sous des climats secs et saisonniers. La végétation adopte un schéma saisonnier comme le montrent des études de terrain localisées, mais son importance et son étendue sont à peine connues. La récente mission Sentinel-2 offre de nouvelles opportunités pour suivre la phénologie de la végétation depuis l'espace.

Le premier objectif de cette étude était d'évaluer le potentiel des données Sentinel-2 pour suivre la saisonnalité de la végétation en Afrique centrale. L'utilisation des données Sentinel-2 visait à répondre aux questions suivantes : quelle est la saisonnalité des forêts d'Afrique centrale, et comment ce fonctionnement saisonnier est-il lié à la saisonnalité des précipitations en République centrafricaine (Mbaïki) et en République démocratique du Congo (Luki) soumises à des régimes pluviométriques inversés. Ce travail s'est appuyé sur trois types de données: (i) les images Sentinel-2, (ii) les données au sol consistant en observations régulières des phénophases et (iii) les données pluviométriques de la mission "Global Precipitation Measurement".

Les séries temporelles de précipitations et d'"Enhanced Vegetation Index" qui en résultent ont permis respectivement de détecter le démarrage des pluies et le début de la saison. Le début de la saison a ensuite été comparé aux observations de terrain. Une analyse supplémentaire des ondelettes a été effectuée sur le site de Mbaïki pour déterminer la fréquence et le moment des événements périodiques de végétation.

Ce travail a démontré l'adéquation des données Sentinel-2 récemment disponibles pour le suivi de la dynamique de la végétation lorsque l'ennuagement reste raisonnable. En outre, les cycles annuels de végétation ont dominé sur les sites étudiés, en lien avec la saisonnalité des précipitations. La comparaison entre les sites a confirmé une inversion de la saisonnalité de la végétation de Mbaïki à Luki en réponse à des régimes pluviométriques inversés de part et d'autre de l'Equateur. À Mbaïki, en moyenne, le signal de la forêt était 16,9 $\pm$ 4,4 jours avant le signal des précipitations, ce qui supporte le contrôle ultime des précipitations. En revanche, pour les deux sites d'étude, le démarrage le plus précoce des précipitations a entraîné le début le plus précoce de la saison en 2019, soutenant l'hypothèse des précipitations comme facteur proximal.

En conclusion, les données Sentinel-2 sont adaptées au suivi de la saisonnalité de la végétation mais nécessiteraient la combinaison avec des images supplémentaires pour faire face aux zones continuellement ennuagées.

Mots-clés: Télédétection, Phénologie, Sentinel-2, Forêts tropicales, Afrique centrale, 'Enhanced Vegetation Index'.

Contents

List of Figures

List of Tables

List of acronyms

AVHRR: Advanced Very High Resolution Radiometer
CR_{SWIR}: Continuum Removed ShortWave InfraRed index
DEM: Digital Elevation Model
EVI: Enhanced Vegetation Index
ESA: European Space Agency
GPM: Global Precipitation Measurement
HLS: Harmonized Landsat-Sentinel-2
IMERG: Integrated Multisatellite Retrievals for GPM
ITCZ: Inter Tropical Convergence Zone
JAXA: Japan Aerospace Exploration Agency
$mNDVI_{705}$: modified red-edge Normalized Difference Vegetation Index
MODIS: Moderate-resolution Imaging Spectroradiometer
NDVI: Normalized Difference Vegetation Index
NIR: Near Infra-Red
NASA: National Aeronautics and Space Administration
RAM: Random Access Memory
SAR: Synthetic Aperture Radar
SOR: Start Of Rain
SOS: Start Of the Season
STRM: The Shuttle Radar Topographic Mission
SWIR: Short-Wave Infra-Red
TRMM: Tropical Rainfall Measuring Mission

Chapter 1

Introduction

1.1 Background

The current decline in biodiversity occurs at an unprecedented rate since the last mass extinction 65 million years ago and is considered as the 6^{th} mass extinction (Ceballos et al., 2015). In this regard, tropical forests are crucial as they harbour 70 to 90 per cent of the terrestrial biodiversity (Myers, 1996). Despite their significant importance in terms of ecosystem functions and services, anthropogenic pressures threaten tropical forests (Malhi et al., 2014). Substantial changes in land use, biotic species (invasion, extinction), biogeochemical cycles and the climate system have led to the recognition of a new geological era: the Anthropocene (Lewis et al., 2015).

Phenology is one of the 20 Essential Biodiversity Variables, developed by the Group on Earth Observations Biodiversity Observation Network (GEO BON, 2017) to monitor the response of individuals, populations and communities to climate change. Under modified climatic conditions, the recurrent vegetation development cycles such as leaf flushing and shedding, flowering and fruiting, named phenology (Bush et al., 2017), is likely to shift in timing (Menzel and Fabian, 1999; Fu et al., 2015; Yu et al., 2017). Global warming implies irreversible changes in ecosystems, which further feedback the rate of climate change.

At present, models agree that tropical phenology is expected to change in the future (Cleland et al., 2007) although the expected responses of tropical vegetation to climate variability are still unclear in the scientific community. Phenological studies in the tropics are relatively recent compared to temperate ecosystems, as tropical ecosystems have long been considered stable systems with little variability in climate and phenology (Abernethy et al., 2018). There is however a diversity of phenology strategies (Newstrom et al., 1994, Sakai, 2001) and responses to climate change. Huete et al. (2006) showed in their study from 2000 to 2005 over the Amazon, an abnormal increase in greenness in response to drought

using remote sensing data while models and flux tower suggest browning vegetation (i.e. a decline in canopy photosynthesis). A first and key step before being able to predict any long-term impacts of climate change is to monitor and assess the current seasonal functioning of tropical forests.

1.2 Tropical phenology

Tropical forests are characterised by high species richness distributed in multi-layered canopies going from emergent trees in the top canopy to shade-tolerant species and C3 grasses in the understory (Ratnam et al., 2011). The extent of tropical forests is bounded between the tropics where the temperatures lie above 15°C all year long (Pan et al., 2013). Annually, tropical forests may experience a dry season that spatially varies in length and intensity. The rainfall seasonality is driven by the Inter-Tropical Convergence Zone (ITCZ) (Siebert, 2014) which is the meeting point of trade winds resulting in a band of clouds and high precipitation near the Equator. The ITCZ follows a seasonal pattern attracted to areas that receive the most solar heating (Yan, 2005) that varies annually according to the orbit position of the Earth. In January, the ITCZ lies about 15S over South America and Africa. In July, it lies at about 25N over Africa and about 30N over Asia (Yan, 2005, Figure 1.1).

During the annual dry season, deciduousness is an evolutionary strategy adopted by some tropical trees to cope with water shortages (Santiago et al., 2016). In this regard, Guan et al. (2015) identified a minimum annual precipitation threshold of approximately 2000 mm yr^{-1} for leaves to persist during the dry season in tropical rainforests worldwide.

In temperate ecosystems, strong changes in temperature and day length from one season to another trigger phenological events resulting in annual phenophases for the majority of species. In opposition, the tropical climate offers the ability for plants to grow and reproduce at any time of the year in the majority of tropical regions (Menaut et al., 1995); Bush et al., 2017; Adamescu et al., 2018). Therefore, tropical forests display a wide diversity of phenological strategies (Newstrom et al., 1994; Sakai, 2001) that vary spatially and temporally (Wright and Calderón, 2006 in Panama; M. E. Brown et al., 2010 in Africa; Angoboy Ilondea et al., 2019 in Democratic Republic of Congo) and between and within species (De Bie et al. 1998 as cited in Ryan et al., 2017). The diversity of tropical phenology patterns has been summarized into four groups by Newstrom et al. (1994): supra-annual, annual, sub-annual and continuous. Newstrom et al. (1994) also underlined that geographic variability in phenological patterns is more likely to occur in the tropics than in temperate regions due to high phenological diversity. In addition, tropical systems exhibit dense canopies, very high species diversity and sophisticated structures that exacerbate the complexity of their spatio-temporal dynamics. The intrinsically simpler functioning coupled with the larger occurrence of long-term datasets of temperate phenology explains the preponderance of phenological studies on temperate forests (Bush et al., 2017).

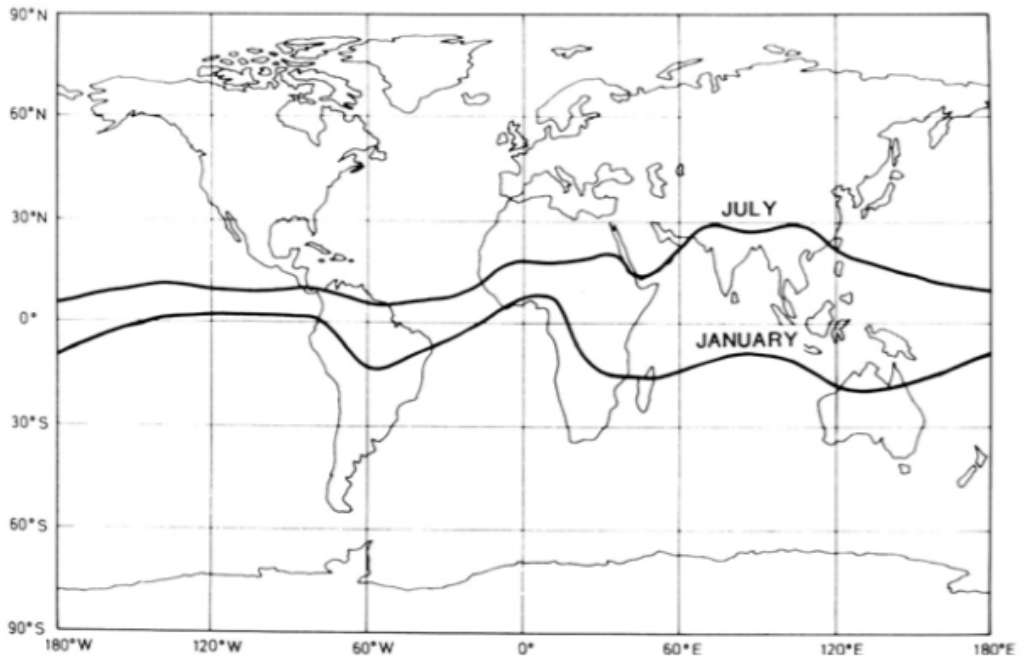

Figure 1.1: Mean locations of the Intertropical Convergence Zone (ITCZ) around the globe in January and July, from Robinson and Henderson-Sellers (1991) according to Yan (2005).

Gradually, phenology studies were extended through tropical areas around the 1970s, with a major focus on flowers and fruits related to the study of animal diet. Mainly because of their importance in terms of wildlife and their easier observation compared to the acquisition of information on leaf phenology in semi-evergreen or evergreen forests (Alberton et al., 2017 as cited in Abernethy et al., 2018). In the 1990s, tropical phenology gained scientists' interest after the proven impact of climate change causing rapid and considerable shifts in temperate phenology (Abernethy et al., 2018). In 1993, Tutin and Fernandez determined that minimum temperature could trigger flowering and fruiting events in Gabon. Progressively researchers began to focus on deciduousness and several environmental cues have been reported to affect leaf phenology. In 1994, Wright and Van Schaik underscored the concordance of leaf flushing with the peak of irradiance when water is available in tropical forests. Current knowledge highlights sunlight (Huete et al., 2006), rainfall seasonality and inter-annual variability (Gond et al., 2013; Guan et al., 2015) as key factors triggering the onset of leaf flushing and shedding in tropical forests (Philippon et al., 2019).

1.3 Central African phenology

Central Africa is one of the most understudied areas of the world (Philippon et al., 2019) and studies focusing on the tropical forests of the Congo basin are even rarer (Verbeeck et al., 2011). The lack of robust long-term ground-based observations of tropical phenology (Adole et al., 2016; Abernethy et al., 2018; Bush et al., 2020) and *in situ* climatic measurements (Washington et al. 2013 as cited in Philippon et al., 2019) make it difficult to monitor and

understand the processes influencing phenology.

In Africa, the main biomes' distribution is related to the length of the dry season (Figure 1.2). Tropical forests in Africa are found under drier and more seasonal climates than the other tropical regions (Guan et al., 2015) and most tropical forests are below the threshold of 2000 mm yr^{-1} (Philippon et al., 2019; Guan et al., 2015). As a result, the water carried over from the preceding wet season may not be sufficient to meet the dry season needs and is a limiting factor for plant photosynthetic activity (Guan et al., 2015). In response to unfavourable conditions, tree growth can be paused by leaf shedding for deciduous trees. Though, deciduousness is not evenly distributed across the forest area (Ouédraogo et al., 2016; Réjou-Méchain et al., 2021) but shows a clear spatial pattern in Central Africa, with more evergreen forest in wet and coastal areas (Atlantic Central Africa) and more semi-deciduous forest covering vast areas further inland (Bouvet et al., 2018, Réjou-Méchain et al., 2021). Beyond the Equator, the majority of forests are found to be semi-deciduous to deciduous alongside the increasing length of the dry season.

Rainfall is not the single driver of the leaf shedding and flushing events. Light is reported in the literature as the main factor, at the same level as water availability in the tropics (Van Schaik et al., 1993; Wright and Van Schaik, 1994). In Gabon, despite a precipitation level below the 2000 mm yr^{-1} threshold, evergreen forests are maintained. Philippon et al. (2019) link the persistence of leaves in the canopy by the reduction of water demand in the dry season owing to a light-deficient climate. Specifically, the high degree of cloud cover during the dry season limits evapotranspiration. Geology has also been highlighted as a determinant of tropical forest deciduousness in the Sangha River Interval by Ouédraogo et al. (2016). In their study, they showed that the relationship between rainfall level and deciduousness is mediated by the geological substrate.

Diverse spatial and temporal vegetation dynamics emerge in response to the above-described factors. The regional extent and timing of the vegetation response to environmental variables are still vague and poorly documented. Yet, an annual seasonal functioning was demonstrated for flowering in a cross-site analysis from Adamescu et al. (2018). The dominance of annual cycles in flowering in tropical Africa was confirmed by Ouédraogo et al. (2020) using herbarium data. However, the considerable intra-specific and inter-annual variation in phenology behaviour was underpinned by Bush et al. (2017) in Lopé, Gabon. The complexity and inter-individual variation in flowering and fruiting patterns in different study sites in Africa was further highlighted by Adamescu et al. (2018). More recently, Réjou-Méchain et al. (2021) were able to map forest types at a regional scale based on species composition but also deciduousness in Central Africa. Progress is underway, but further research on understanding the functioning of the semi-deciduous forests is still needed.

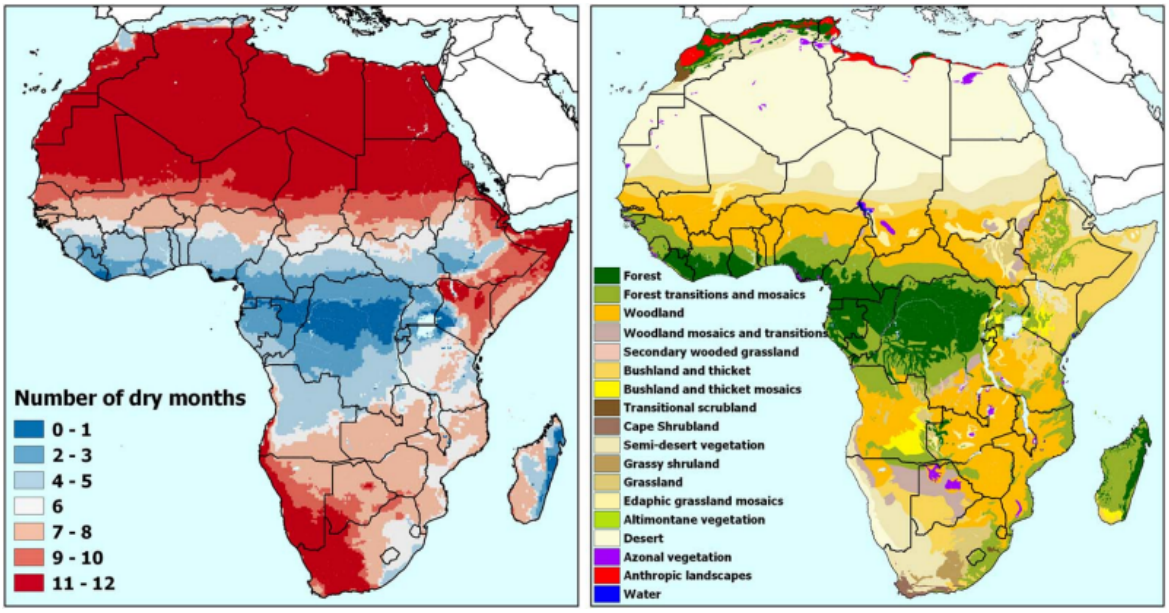

Figure 1.2: Paralleling biomes distribution to dry season length in Africa. Taken from Bouvet et al. (2018).

1.4 Land surface phenology

Satellite remote sensing offers the opportunity to undertake large-scale studies allowing spatial comparisons and improving the knowledge on tropical phenology. In particular, leaf phenology can be captured by optical remote sensors through vegetation indices and greenness proxies based on the reflectance properties of the leaves (Helman, 2018). Such studies using space-borne optical sensors at a regional to global scale are named land surface phenology (Helman, 2018). Time-consuming and expensive ground observations, which record the different phenophases of individual trees, are generally difficult to maintain over the long term. In contrast, the simultaneous monitoring of vegetation phenology on different landscapes is possible at a moderate cost with satellites. Optical data at coarse to medium spatial resolution and high temporal frequency are subject to a growing use to monitor tropical forests' canopy. Several studies were able to monitor leaf phenology through optical remote sensing, mainly in Amazonia (Asner et al., 2000; Xiao et al., 2006; Silva et al., 2013) in Monsoon Asia (Huete et al., 2008; Suepa et al., 2016) and in Africa (Adole et al., 2018). Researchers largely depend on open access products and first call on Landsat data, starting the vegetation monitoring from space (Henebry and de Beurs, 2013). Then, products moving from Advanced Very High Resolution Radiometer (AVHRR) to Moderate-resolution Imaging Spectroradiometer (MODIS) sensors prevailed. The commonly used information retrieved in land surface phenology is the start of the season, end of the season and peak of the season (Misra et al., 2020).

Despite the promising results in capturing leaf phenology by remote sensing products, some shortcomings lead to misinterpretation of observed trends (Helman, 2018). First, the signal acquired from a spaceborne sensor is influenced not only by vegetation properties but also by multiple other factors. Lange et al. (2017) state that "these effects include atmo-

spheric interference, snow cover, soil-wetness, viewing geometry and illumination conditions as well as the distorted signal under overcast conditions". In addition, the studies of Morton et al. (2014) and Huete and Saleska (2010) both revealed that artefacts from changes in sun sensor geometry could lead to a wrong interpretation of the vegetation indices. For instance, a green-up was observed during drought conditions over the Amazonian forest (Morton et al., 2014). Secondly, the intrinsic nature of leaf phenology is rapid and dynamic (Longman and Jenìk, 1974) implying frequent observation in order to capture the phenological events. However, cloud cover contamination occurs frequently with optical sensors limiting the acquisition of images. The minimum number of images required to accurately capture phenological events depends on the timing and availability of cloud-free images and the vegetation type studied (Zeng et al., 2020). In the tropics, cloudiness and haze are highly persistent (Asner, 2001) and result in a lack of good quality images. Temporal resolution is therefore a key factor to monitor vegetation seasonality. Thirdly, mixed pixels are recurrent in land surface phenology studies (Lange et al., 2017) and refer to the possibility that a single observation point may or may not represent the overall pixel characteristics (White et al., 2009) because of heterogeneous landscape and complex multi-canopy layers systems (Helman, 2018). To limit this adverse effect, a fine spatial resolution is required. There is thus a trade-off between temporal and spatial resolution when using a single satellite time series as the data source (Zeng et al., 2020).

The recent launch of the Sentinel-2 satellite by the European Space Agency (ESA) is promising to overcome those limitations by providing high-resolution (10-30 m depending on the spectral band, Figure 1.3) multispectral data with a temporal resolution of up to five days. The Sentinel-2 mission arises to ensure the data continuity and improve the performance of earlier missions such as Landsat and SPOT (ESA, 2015a). Sentinel-2 consists of a twin-satellite system designed to provide data for land monitoring, emergency management, security purposes and climate change assessment (ESA, 2015a). In particular, data acquired from this mission provide geographical information on land cover and related variables such as vegetation state via the assessment of biogeophysical parameters. The first sensor (Sentinel-2A) acquires images since 2015 while the second (Sentinel-2B) was launched in 2017. Therefore, the Sentinel-2 mission provides new opportunities to monitor land surface phenology at high spatial resolution and high revisit frequency. With five years of data, the use of the Sentinel-2 sensors has gained importance in terms of plant phenology studies (Misra et al., 2020). Below are presented a non-exhaustive list of studies building Sentinel-2 time series, either alone or combined with other datasets for several purposes such as:

(i) To map and monitor croplands dynamics. For instance, Veloso et al. (2017) and more recently Meroni et al. (2021), investigated the temporal behaviour of crops using sentinel-1 and -2 data. Both Mercier et al. (2020) and d'Andrimont et al. (2020) assessed the potential of using sentinel-1 and -2 data to identify the phenological stages of the rapeseed. In 2020, Liu et al. developed an algorithm used to map cropping intensity in China by combining Landsat, Sentinel-2 images and Google Earth Engine.

(ii) To monitor grasslands. Vrieling et al. (2018) retrieved vegetation phenology of grasslands and maize based on Sentinel-2 time series. Both Pastick et al. (2020) and Griffiths et al. (2020) characterised land surface phenology from Landsat and Sentinel-2 time series.

(iii) To map wetlands. Mahdianpari et al. (2019) and Cai et al., 2020 used Sentinel-2 time series to map wetlands respectively in Newfoundland and in the Dongting Lake wetland.

(iv) To characterise the phenological dynamics of urban areas as in a study of Granero-Belinchon et al. (2020).

(v) To map and monitor forest species. For instance, Grabska et al. (2019) mapped the mosaic of the forest species in the Polish Carpathian Mountains. The monitoring of boreal forest phenology was performed by Jönsson et al. (2018). In contrast, Lange et al. (2017) and Kowalski et al. (2020) used Sentinel-2 data to monitor the phenology of temperate species.

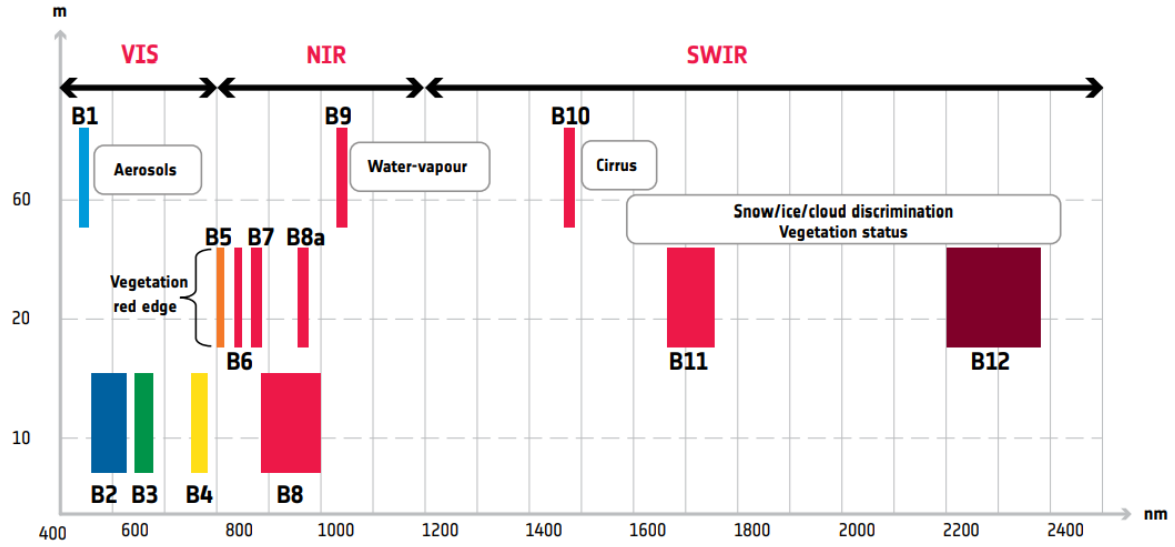

Figure 1.3: Spatial resolution versus wavelength. Sentinel-2's 13 spectral bands covering the visible and the near-infrared to the shortwave infrared and their respective field of application. The spatial resolution is 10, 20 or 60 m; taken from: ESA (2015b).

1.5 Aims

Despite their crucial importance, phenology studies in Central Africa are rare and lead to a lack of knowledge on the importance and extent of the seasonal functioning of vegetation. Using remotely sensed data is an opportunity to cope with the lack of field measurements. Few studies have exploited the potential of the Sentinel-2 mission to understand the seasonality of African tropical forests, and how is this seasonal functioning related to rainfall seasonality.

The main objective of this work is to assess the potential of Sentinel-2 data to monitor vegetation seasonality in Central Africa through the development of a workflow for the processing of Sentinel-2 data. The method will be calibrated based on a first study site located in the Central African Republic (Mbaïki). At this stage, the link between the vegetation seasonality and the rainfall pattern will be investigated. In a second step, the method will be applied to a second study site, in the southern hemisphere (Luki). The aim is twofold. Firstly, to determine the possibility of using sentinel-2 data to carry out multi-site studies. Secondly, to highlight the influence of different rainfall regimes on vegetation dynamics.

The questions below will be specifically addressed:

(i) Are Sentinel-2 data suitable to monitor the vegetation seasonality in Central Africa?

(ii) What is the vegetation dynamics in Mbaïki and Luki?

(iii) What is the influence of the rainfall regime on the vegetation seasonality in Mbaïki and Luki?

This study should result in a methodology that consists of a powerful tool for undertaking multi-site studies.

Chapter 2

Material and methods

This section aims to give an overview of the study sites, describe the data used and finally present the method developed and implemented. This work relies on three data types:(i) Sentinel-2 data, satellite images collected in the frame of the Sentinel-2 mission, (ii) ground data collected in Mbaïki and in Luki consisting of regular observations of different phenophases (flowering, fruiting, leaf flushing and shedding) in tree crown, (iii) satellite rainfall data from the Global Precipitation Measurement Mission (GPM).

2.1 Study sites

Two study sites from the two hemispheres were considered. The first one (Mbaïki) was used to calibrate the approach while an additional site (Luki) was used to carry out a cross-site comparison on both side of the Equator (Figure 2.1 a). For each site, the study focuses on a frame of 25 x 25 km^2 marked in Figure 2.1b) and c) as black frames.

The first study site is located nearby the city of Mbaïki (3°52'N, 17°59'E) in the Lobaye Province, Central African Republic (Figure 2.1). Mbaïki is located at the northern margin of the Congo Basin. The climate is humid tropical and seasonal with three months dry season from December to February accumulating 84.5 mm of rainfall (Figure 2.1b). The mean annual precipitation is equal to 1636 mm[1] (Figure 2.1a). The soil type is classified as Ferralsol by the World Reference Base for Soil Resources soil classification (WRB, IUSS Working group, 2014). The vegetation consists of a mix between semi-deciduous forests and savanna (Gourlet-Fleury et al., 2013, Ouédraogo et al., 2011).

The second site corresponds to the Luki Man and Biosphere Reserve in the Province of Bas-Congo, Democratic Republic of Congo (Figure 2.1a). The Luki Reserve is considered

[1]Rainfall data source: GPM data (G. Huffman et al. (2019)). Temperature data source: National Oceanic and Atmospheric Administration (NOAA).

representative of the Mayombe forest (Lubini, 1997 cited in Angoboy Ilondea et al., 2019) and gathers a semi-deciduous forest (Angoboy Ilondea et al., 2019) growing on ferralitic soil. The rainfall seasonality is unimodal with a strong dry season from June to September and 12.2 mm[1] of accumulated rainfall (Figure 2.1c). The dry season in Luki is stronger compared to Mbaïki in terms of both intensity and duration.

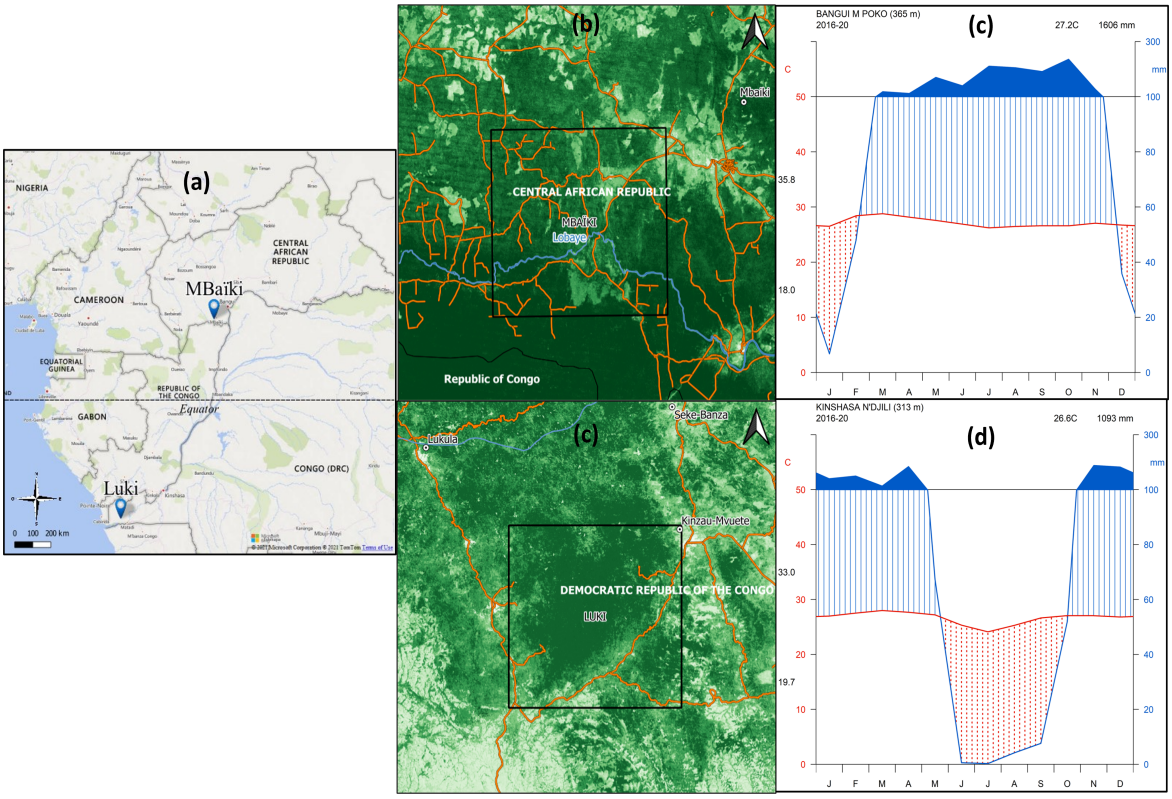

Figure 2.1: (a) Location of the study sites in Central Africa. The northern blue pin locates the Mbaïki forest experiment (in a logging concession) on the upper part of the Equator. The southern blue pin locates the Luki reserve on the lower part of the Equator. Basemap: ©Bing.(b) and (c): Mbaïki and Luki study sites marked as a black frame on the basemap of tree cover (0-100 %, Hansen et al. (2013)). The roads and rivers are coloured respectively in orange and blue. (d) and (e): Walter and Lieth diagram over from 2016 to 2020 respectively for Mbaïki and Luki. The red line represents the mean monthly temperature, the blue line the mean monthly rainfall. The dry season is represented by the dotted area, the humid period by vertical hatching. When the monthly rainfall is greater than 100 mm, the scale is increased from 2mm/ºC to 20mm/ºC. Rainfall data source: GPM data (G. Huffman et al. (2019)). Temperature data source: National Oceanic and Atmospheric Administration (NOAA).

2.2 Ground data

One of the major challenges in land surface phenology estimation in Africa is ground validation (Adole et al., 2016) although important to interpret them adequately and reliably.

In the Mbaïki Experimental Station (3°90'N, 17°93'E), 14 different species from five botanical families are monitored since 2005. Among them, 12 are deciduous. The most represented species is *E.cylindricum* with 125 individuals followed by *T.scleroxylon* with 114 individuals. The dataset consists of crown observations from the ground taken at a 15 days

frequency for trees located within ten plots of four hectares. The plots are monitored since 1982 while the dominant phenophase for these trees is reported since 2005 by a single person present on site (Fidèle Baya). The field reports provide the day of year corresponding to the leaf shedding while leaf flushing cannot be captured because of it coexistes with flowering (considered as the dominant phenophase). In 2007, new trees were added to enlarge the species diameter range. In 2013, the phenology monitoring was interrupted due to socio-political troubles in the country. In the frame of this work, the seasonal vegetation behaviour is retrieved from the ground datasets at the 2007-2013 and 2016-2018 periods.

In the Luki Man and Biosphere Reserve, the phenology was monitored from 1947 to 1958 by the same field team. The number of monitored species reaches 158 among which 52 are deciduous. The most represented species are *P.balsamifera* with 194 individuals, followed by *T.superba* with 184 individuals. The phenological data were taken at a frequency of 10 days along six paths (Angoboy Ilondea et al., 2019). In Luki, the ground data are used to give an overview of the yearly dynamic of the trees given the non-concordance of the field data (1947-1958) and the remote sensing images (2015-2020).

In both cases, a tree is defined as defoliated when the field worker considers the tree to be completely leafless.

2.3 Rainfall data

The precipitation dataset came from the Global Precipitation Measurement (GPM) mission. This mission is based upon the success of the Tropical Rainfall Measuring Mission (TRMM). The National Aeronautics and Space Administration (NASA) and the Japan Aerospace Exploration Agency (JAXA) launched the TRMM in 1998. TRMM data are widely used by scientists to investigate climate drivers of tropical phenology in Africa (Zhang et al., 2005, Philippon et al., 2016, Ryan et al., 2017, Guan et al., 2015, Philippon et al., 2019). In 2019, Camberlin et al. compared several satellite-based rainfall products (ARC, CHIRPS, CMORPH, PERSIANN, TAPEER, TARCAT, TRMM) in Central Africa. Their study revealed that TRMM products perform the best rainfall estimation for the mean monthly rainfall regimes and daily rainfall over Central Africa.

Following the widespread use of the TRMM mission, the NASA and the JAXA build up an advanced network of satellites as part of the Global Precipitation Measurement (GPM) mission in 2014 (Hou et al., 2014). The GPM core observatory aims to provide a continuous record from the TRMM as well as additional and advanced information on precipitation characteristics (G. J. Huffman et al., 2020). The GPM core observatory spacecraft gathers cutting-edge sensors allowing to include light-intensity precipitation and falling snow measurements (Hou et al., 2014). In the literature, the GPM products are often referred to as the Integrated Multisatellite Retrievals for GPM (IMERG) products. IMERG is a

multisatellite algorithm developed by the NASA that "intercalibrates, merges, and time-interpolates "all" satellite microwave precipitation estimates in the GPM constellation, then incorporates microwave calibrated infrared satellite estimates and precipitation gauge analyses" (G. J. Huffman et al., 2020)". Dezfuli et al. (2017) assessed the evolution of the quality of IMERG products compared to its predecessor TRMM over Africa. They showed that IMERG performed better than TRMM to capture the diurnal cycle while the annual cycle is not significantly better depicted for IMERG although they both show reasonable results.

For this work, data for the 2015-2020 period were downloaded freely on the GES DISC platform (NASA) at a temporal and spatial resolution respectively of 1 day and 0.1°x 0.1°. The daily accumulated rainfall was averaged over the 4 pixels of each study area given the low spatial variation between the pixels.

2.4 Preprocessing of Sentinel-2 data

This section details primarily the Sentinel-2 data and preprocessing (Figure 2.2). The preprocessing consists in the images selection and download and then how to transform the raw physical variables measured by the space-born sensors (reflectance in different wavelengths) into greenness proxies in the form of vegetation indices. All the data were processed in RStudio 1.4.11.06 using R4.0.4.

The first Sentinel-2 satellite was launched in June 2015 with a revisit frequency of 10 days at the Equator and in the absence of clouds, rising to 5 days with the entry of the second satellite in March 2017. The data description is presented in Table 2.1. The spatial resolution depends on the spectral band (Figure 1.3). The relevant bands to monitor vegetation are the spectral bands in the visible domain corresponding to blue, green and red channels (B02, B03, B04), three red-edge bands (B05, B06, B07), a Near Infrared (NIR) broadband (B08), a NIR narrow band (B8A), and two Short-Wave Infrared (SWIR) bands (B11 and B12) (Figure 1.3).

Table 2.1: Characteristics of Sentinel-2's products available on the Copernicus Open Access Hub platform. TOA (Top-of-atmosphere), BOA (Bottom-of-atmosphere) adapted from ESA (2015a).

Type	Description	Format
Level-1C	Non corrected data: TOA reflectances in cartographic geometry	orthoimages: 110 x 110 km^2 in UTM/WGS84 projection
Level-2A	Corrected data: BOA reflectances in cartographic geometry	orthoimages: 110 x 110 km^2 in UTM/WGS84 projection

2.4.1 Images selection

Before 2017 and the launch of the second Sentinel-2 satellite, the theoretical revisit frequency was 10 days. After this date, a mean of one image every five days is reached. To reduce the downloading time, a preliminary step of images selection was performed. Two different approaches were successively implemented on the Mbaïki site to retrieve the land surface phenology time series.

(i) Approach 1: by selecting cloud-free images, this approach aims to have a high-quality dataset. It allows having a high degree of confidence in the data produced and avoids misinterpretation. It reduces considerably the download and computational time as well as the disk space used. The first selection step consisted of filtering of the images having a cloud coverage constrained below 30 % on the Sentinel-2 tile of interest. For all the data fulfilling this criterion, a visual classification in four distinct classes was made based on the preview images available on Sentinel Playground. From A: very high quality to D: mediocre quality. The D class images are then removed resulting in a dataset of 84 images. Some products provided are defective (corrupted zip files). Therefore, a last filtering of the resulting images was made (from 84 to 80 images). The 80 images list were used as input for the downloading step.

(ii) Approach 2: this approach aims to gather a large number of data regardless of the quality. It allows monitoring at a higher time resolution required to capture the quick phenology changes. In this case, images were removed from the dataset in case of a defective zip file or of a 100 per cent cloud cover. It led to an amount of 261 images.

The first approach resulted in a large number of data gaps leading to large time spans between two images. However, the leaf shedding and flushing is rapid and dynamic and requires a high frequency of observations. The results produced by approach 1 could not be interpreted adequately. The second approach was then preferred for both sites.

2.4.2 Download

Sentinel-2 tiles can be downloaded freely on the Copernicus open access hub. However, the oldest and least used Sentinel-2A and B data have been removed from the online ESA archive and stored in the long term archive. It is though possible to request a query of products in the long term archive. The ESA server restores the products online within 24 hours after triggering the retrieval. Nevertheless, the ordering process undergoes failures quite often. In addition, only two concurrent downloads are allowed on the Copernicus open access hub. Finally, no automatic download is initiated when the products are available.

Regarding the high amount of images needed to build a consistent time series, a manual

download of the images is not efficient. The R toolboxes (sen2r, getSpatialData) tested to order and download the data through the ESA server resulted in recurrent failure when ordering the images from the ESA server to retrieve long term archive products.

Therefore, the retrieval and download of Sentinel-2 data were made through the French access to sentinel products, PEPS (Figure 2.2). The main advantages are the quick data availability and reliability compared to the ESA server. Manually, the images in a given time range and for a tile of interest were selected and put in a cart on PEPS. Then a file with a .cart extension was downloaded and used as input of the peps downloader app. Automatically, when the images are online, peps downloaded the zip file containing the data and metadata. Afterwards, the zip files were unzipped and put in the input folder ready to be corrected by an automated R script.

2.4.3 Correction

The ESA developed a prototype processor called sen2cor that performs atmospheric, terrain and cirrus correction and a scene classification (ESA, 2018). The algorithm takes as input the Level-1C images and a raster representing the topography (Digital Elevation Model (DEM)). The Shuttle Radar Topographic Mission (SRTM) 90 m Digital Elevation Data located on the study site of interest is downloaded freely on The CGIAR-CSI GeoPortal. The version sen2cor 2.5.5 was used for data before 2017 and the updated and faster 2.8.0 version for ulterior dates acquisitions. The sen2r toolbox developed by Ranghetti et al. (2020) was used to launch the sen2cor algorithm from R ('Apply sen2cor' step in Section 2.2).

2.4.4 Band selection, cropping and resampling of images

In a first step, the required bands (B02, B03, B04, B05, B06, B07, B08, B8A, B11 and B12) were selected. In addition, the cloud mask based on the scene classification band produced by sen2cor was retrieved. At this step of the processing chain, the data were still in the form of Sentinel-2 tiles (meaning a 110 x 110 km^2 square). The images were then clipped on the study area extent and resampled to the desired resolution by bilinear interpolation (10 m). Those steps were performed thanks to the *stars* R package. All the bands were then gathered in one raster stacked file.

2.4.5 Compute indices

Numerous vegetation indices based on reflectance in different wavelengths can translate the vegetation status. Among them, the following indices are computed.

The Normalized Difference Vegetation Index (NDVI)

The NDVI, developed by Rouse et al. (1974), has been the most widely VI used in quantifying green vegetation. It is the normalized ratio between green leaf scattering in NIR wavelengths and chlorophyll absorption in red wavelength. Its formula adapted to Sentinel-2 bands is:

$$NDVI = \frac{B08 - B04}{B08 + B04} \tag{2.1}$$

Leaf phenology's characteristics used to be largely depicted through the NDVI. Though, NDVI appears to have some limitations such as saturation in multi-layer closed canopy (Gitelson, 2004 as cited in Henebry and de Beurs, 2013) typical in the tropics. It is also established that the NDVI is sensitive to atmospheric aerosols and soil brightness and colour (Xue and Su, 2017).

The Enhanced Vegetation Index (EVI)

Progressively the EVI replaced the NDVI in land surface phenology to get rid of the limitations appearing in tropical regions. Its calculation is based on the NIR (B08) and RED (B04) bands and its formula is:

$$EVI = 2.5 * \frac{(B08 - B04)}{(B08 + 6.0 * B04 - 7.5 * B02) + 1.0} \tag{2.2}$$

The modified red-edge Normalized Difference Vegetation Index ($\mathbf{mNDVI_{705}}$)

In areas with high plant species diversity and functionality, vegetation indices tend to be poorly correlated with chlorophyll content, mainly due to leaf surface reflectance (Sims and Gamon, 2002). The $mNDVI_{705}$ was developed based on the NDVI705 by Sims and Gamon (2002) to reduce the effect of differences in leaf surface reflectance that appeared. This index displays a great sensitivity for high chlorophyll content.

The $mNDVI_{705}$ uses the vegetation red-edge band (B06) in its formula showed in Equation 2.3. The red-edge band is particularly sensitive to biophysical parameters of forests (Zhu et al., 2017).

$$mNDVI_{705} = \frac{B06 - B05}{B06 + B05 - 2 * B02} \tag{2.3}$$

The Continuum Removed ShortWave InfraRed index ($\mathbf{CR_{SWIR}}$)

The SWIR band domain includes broad water absorption features. The CR_{SWIR} takes advantage of this sensitivity to vegetation water and reacts positively with a decrease in leaf

water content.

$$CR_{SWIR} = \frac{B11}{B8A + (\lambda_{B11} - \lambda_{B8A}) * \frac{(B12 - B8A)}{(\lambda_{B12} - \lambda_{8A})}} \tag{2.4}$$

2.4.6 Cloud and green mask

Clouds and non-vegetated areas such as water and urban surfaces' reflectance do not depict the vegetation response. Therefore, the pixels contaminated by clouds or located in urban or water areas have to be removed. The pixels filtering calls on two raster masks named 'cloud mask' and 'green mask'.

The R code produced an enhanced cloud mask based on the initial cloud mask provided by the sen2cor algorithm and radiometric filtering. The latter eliminates pixels with high reflectance (>5 %) in the blue band (B02) and low reflectance (<20 %) in the NIR band (B08) filtering for suspected clouds and cloud shadows respectively. One cloud mask is associated with each acquisition date.

In opposition, the green mask is common for all the dates and was computed based on an NDVI threshold. To account for recent changes, the NDVI values are taken for the latest cloud-free image. All values below 0.5 are considered urban areas.

For each index and each date, the corresponding cloud mask and the green mask are applied (Figure 2.2).

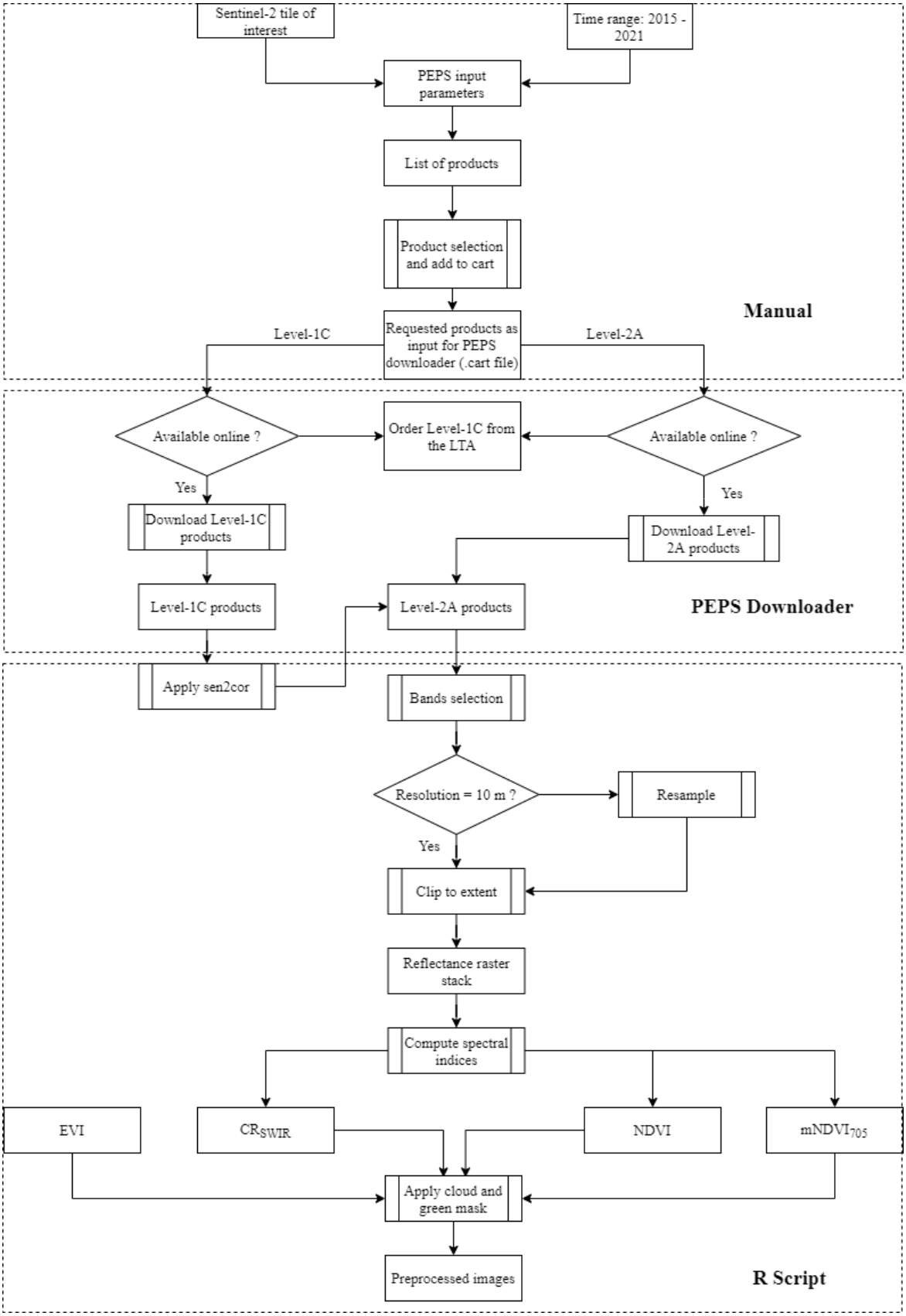

Figure 2.2: Flow diagram of the main downloading and processing steps of Sentinel-2 products implemented to obtain the preprocessed spectral indices.

2.5 Data analysis

After the processing stage, for each date, four raster images corresponding to the four indices (NDVI, EVI, mNDVI_{705} and CR_{SWIR}) consisting of the inputs for the data analysis stage. Below are presented the main analysis performed to validate the method and investigate the link between rainfall and vegetation seasonality.

2.5.1 Land cover classification

The vegetation cover is not uniform across each study site. The sites are mainly covered by forests and savannas, but also by agricultural mosaics and, to a small extent, by roads and villages. Starting on this observation, the tree cover map from Hansen et al. (2013) (Figure 2.3) was used to distinguish the forested pixels (tree cover ≥ 70, Achard et al., 2014) from the non-forested pixels. The latter class, including essentially savannas and less extensively agricultural areas, will be recalled as "non-forest". Both sites harbour a mosaic landscape with a variable percentage of tree cover (Figure 2.3). They are mainly covered by forest with 89.9 % for Mbaïki and 76.9 % for Luki.

In addition, to give an overview of the spatial diversity of species in each study sites, an alpha diversity analysis is performed thanks to the BioDivMapR R package developed by Féret and de Boissieu, 2020. It uses the spectral information to retrieve information on the species diversity.

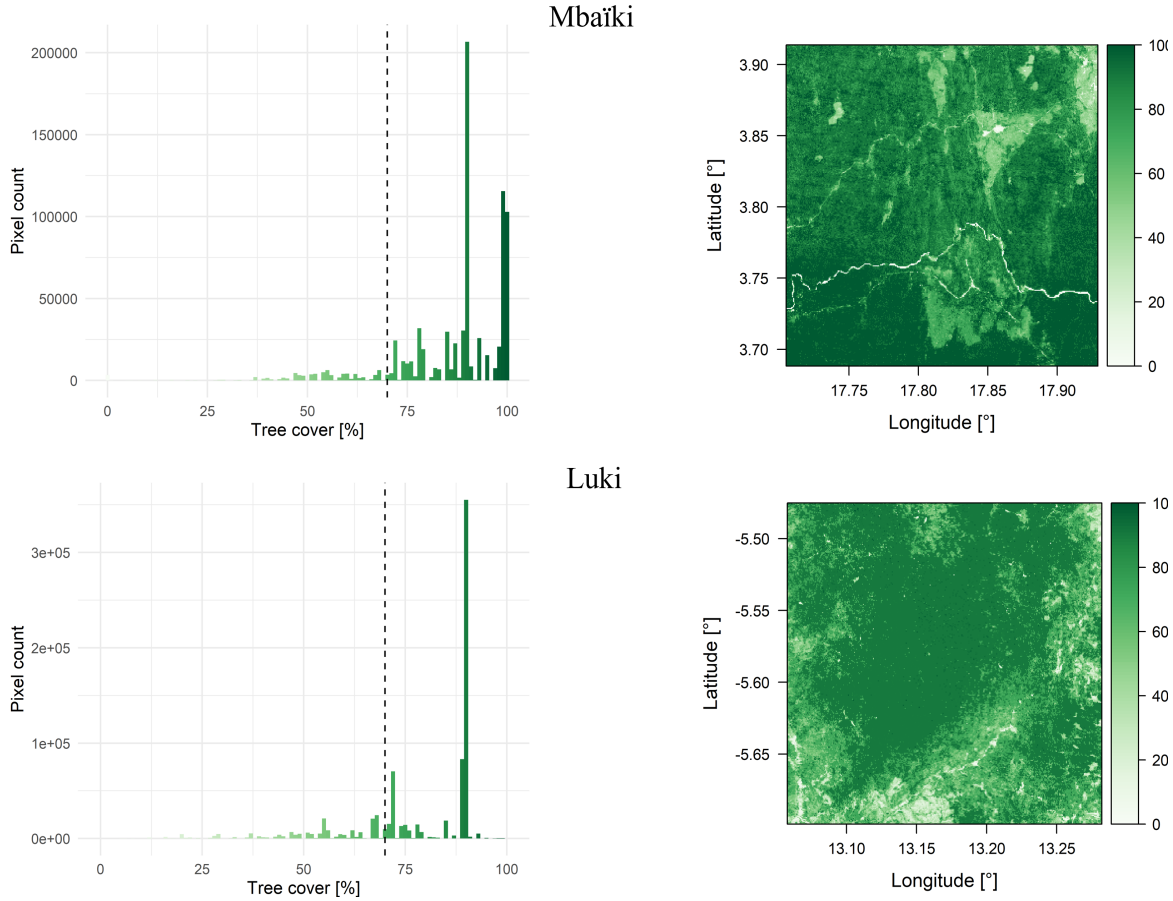

Figure 2.3: On the left: Histogram distribution of the pixels according to the tree cover percentage for Mbaïki and Luki. The vertical dotted line represents the threshold differentiating the forest from the savanna. On the right: Tree cover maps from Hansen et al. (2013) representing the tree cover percentage for Mbaïki and Luki.

2.5.2 Method validation

In a first approach, the purpose is to implement a method to study the vegetation seasonality. The assessment of exploitable results was a preliminary step. Therefore, the pixels' information was aggregated in one mean value for each date, separately for each land cover class. Then, the data were smoothed using a Savitsky-Golay filter. The same approach was applied to rainfall data. Then, the data were summarized to an upper level, the index and rainfall data were monthly averaged over the five years. This method was implemented to the four vegetation indices.

The ground data were used to check the concordance between the main defoliation periods and decrease in vegetation indices. The comparison is then made at a finer scale corresponding to the pixel level. Seventeen regularly defoliated individuals from the highly seasonal *Milicia excelsia*'s species were selected in the ground dataset from Mbaïki. In parallel, the corresponding pixels were extracted from the satellite images as well as the surrounding pixels in a 10 m buffer to account for the entire tree crown. The signal obtained is therefore, the average of the pixels extracted for each individual.

2.5.3 Start Of the Season (SOS) and Start Of Rain (SOR)

The relationship between the vegetation index rise, interpreted as the Start Of the Season (SOS) and the start of the rainy season recalled as the Start Of Rain (SOR) was investigated.

For this purpose, Sentinel-2 data were first adjusted to the spatial resolution of the tree cover percentage from Hansen et al. (2013) used to distinguish forested pixels from non-forested pixels. The Sentinel-2 images were therefore aggregated to 30 x 30 m^2 resolution using a bilinear method. The SOS corresponds to the annual first sharp increase in the vegetation index and was detected based on an adapted method from Archibald and Scholes (2007) (also used in Ryan et al. (2017)). The SOS was defined as the first day that satisfies the following condition:

$$movag_{EVI}(t : t + 3) > movag_{EVI}(t - 10 : t) \tag{2.5}$$

t represents a punctual observation while $movag$ corresponds to the moving average.

The SOS period starts in January and in July respectively for Mbaïki and Luki. The achieved revisit frequency with both satellites is five days, however, cloud cover leads to frequent loss of data. To obtain one value every five days, a linear data gap filling was performed. To reduce the noise of the time series, a smoothing filter (Savitsky-Golay) was then applied. For some pixels, the large amount of gap-filling consequently to data gaps lead to abnormal SOS values occurring on the first day of the SOS period of interest. The seasonal minimum was not captured by the satellites images and the SOS detected first day was not reliable. Thus, those pixels are removed from the analysis.

In the tropics, according to Köppen's climate classification, a month is considered very dry if the amount of rainfall is less than 50 mm (coloured by red dots in Figure 2.1b,c) and very wet when it receives more than 100 mm of rainfall (filled with blue in Figure 2.1b,c). Thus, the end of the rainy season was marked by a threshold of rainfall exceeding 25 mm in 15 days. The beginning of the rainy season was detected for each pixel as the first fortnight with more than 25 mm. The SOR corresponds to the first day of this fortnight.

2.5.4 Frequency analysis

The detection of the most dominant frequencies from vegetation index time series is useful to monitor the vegetation dynamics. Typically, the Fourier analysis has been previously used to determine the dominant frequencies in vegetation index time series and to test for seasonal trends (Azzali and Menenti, 2000, Stöckli and Vidale, 2004, Bush et al., 2017). This approach compares the data with a superposition of basis sine and cosine functions. However, the Fourier analysis does not provide any information on the timing at which the regular events occur. This weakness can be compensated by an enhanced method based

on the Fourier analysis named Windowed Fourier Transform (Martinez and Gilabert, 2009). However, the latter requires stationary time series (Martinez and Gilabert, 2009). This is not the case when dealing with vegetation index time series as they present fluctuations going from the seasonal to long-term time scale (Ben Abbes et al., 2018).

In this context, the wavelet approach presents two main advantages: (i) the absence of the stationary requirement, (ii) the borrowing of three dimensions information: frequency, time and intensity (Moreira et al., 2019). Firstly, the wavelet transform compares the data with local basis functions that are stretched and translated to retrieve respectively the frequency and the timing (Martinez and Gilabert, 2009). Secondly, the wavelet coherence enables the analogy with two different time series by providing information on how two signals co-vary on different scales over time (Percival et al., 2004).

The wavelet transform was applied on the EVI and rainfall time series while the wavelet coherence was used to analyse the rainfall influence on the EVI time series. Both imply setting up some mathematical parameters. The chosen mother wavelet (i.e. the original function stretched and translated to construct the set of basis functions (Martinez and Gilabert, 2009)) was the Morlet wavelet. The statistical significance level of coherence is 0.95. Finally, both techniques require a constant time step between each value. In this case, the chosen time step is 5 days based on the theoretical revisit frequency of the Sentinel-2 satellites. To fulfil this condition, the EVI time series were filled calling on a bilinear interpolation method. Regarding the rainfall, the daily accumulated rainfall was summed over 5 days.

Chapter 3

Results

This chapter first gives an overview of the data for the two study sites. The main results obtained at the first study site (MBaiki) were described as follows: the ground data overview and method validation, then, the vegetation seasonality and the influence of precipitation on vegetation functioning. Less intensively, the results obtained at the Luki study site were presented on the same basis as Mbaïki's.

3.1 Data overview

3.1.1 Spectral species diversity

The results presented in Figure 3.1 correspond to the application of the *BioDivMapR* package on the latest high-quality images for each site. The same spatial patterns were obtained for the dry/wet season (results not shown). Regarding Mbaïki, the highest Shannon index' values were gathered by the forest with a mean ± sd of 2.62 ± 0.31 while the non-forest displayed a lower mean diversity value of 1.93 ± 0.53. The forest values in Luki were slightly lower with 2.34 ± 0.30 but the non-forest values were higher in Luki with 2.12 ± 0.54.

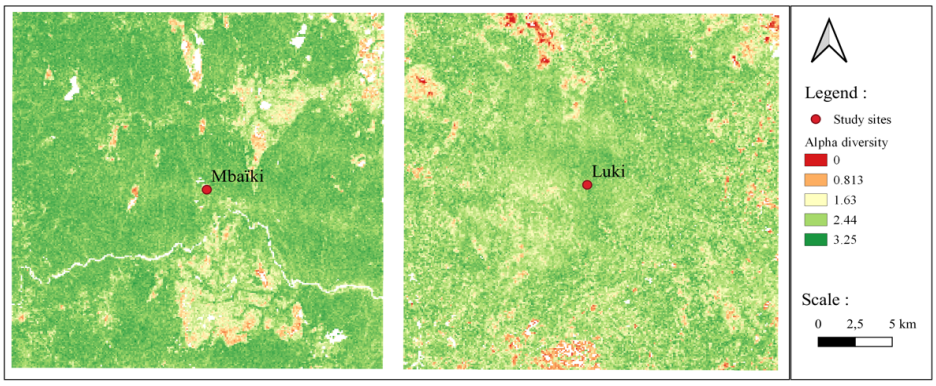

Figure 3.1: Alpha diversity maps: Shannon index over the study areas. On the left: Mbaïki. On the right: Luki.

3.1.2 Temporal resolution

The major impact of the persistent cloud cover and revisit frequency on the data quality is demonstrated by Figure 3.2. Before 2017, given the reduced satellite revisit frequency, the number of images was poor in both study sites. In total, the number of images with more than 50% cloud-free pixels was 84 for the first study site (Mbaïki) and plummeted to only 6 for the second study site (Luki). In addition, on 242 images, 135 did not provide any information (0 pixels available) in Luki. This led to less than half of the data available. In Mbaïki, the average time lapse between two values was 19.9 days before 2017 against 9.3 days after 2017. In contrast, in Luki the average time laps between two values was 36.9 days before 2017 against 15.8 days after 2017. For the two sites, the results prior to 2017 were discarded for further analysis due to the large time gap between two observations.

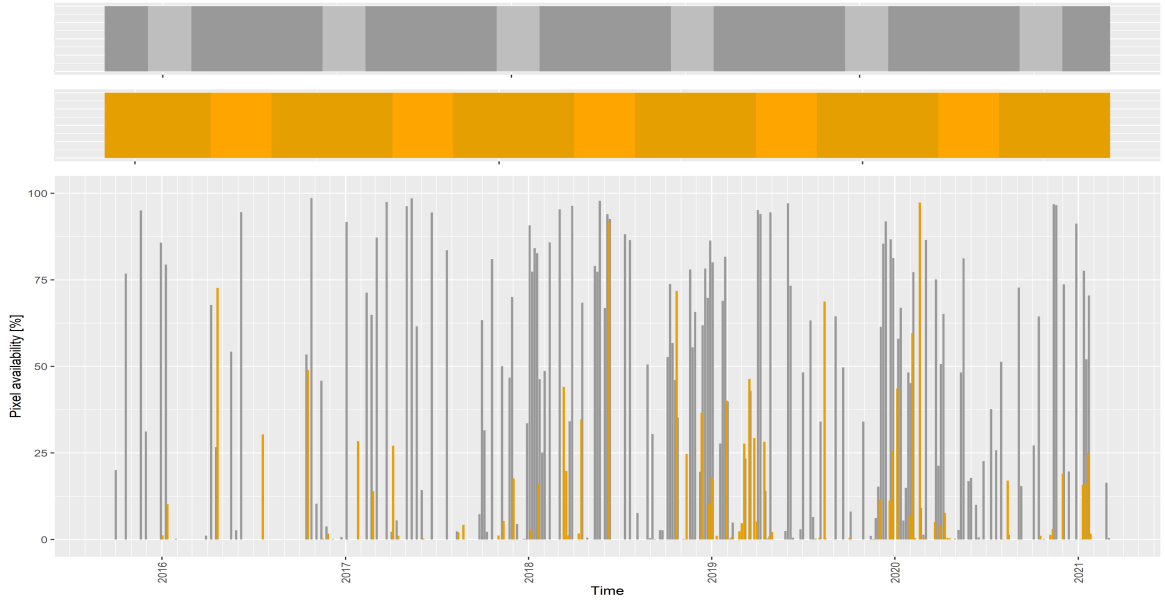

Figure 3.2: Pixel availability i.e. the proportion of cloud-free pixels, according to time. The striped bars represent the alternation dry (light) and wet (dark) seasons. In grey, Mbaïki. In brown, Luki.

3.2 Mbaïki

3.2.1 Ground data and method validation

The ground dataset available in Mbaïki was used to calibrate the approach. The seasonal variation of leaf shedding for the 12 deciduous species is shown in Figure 3.3. On average, the observed defoliation took place mainly around December to February with 7.41 % of the trees defoliated at this period. These defoliation events were in line with the dry season from December to February (Figure 2.1) and observed in the majority of the individuals and two thirds of the species. August showed the second most important percentage of defoliated trees (3.69 %). The August defoliation was mainly observed for *E.angolense*, *E.candolei*,

E.cylindricum and *T.scleroxylon* species which is probably associated with caterpillar predation. September and October were also subject to above-average defoliation for *E.angolense*, *E. candolei* and *K. anthotheca*. Finally, *C.boukokense*'s individuals were deciduous only in September and by a low percentage (0.22 %).

Figure 3.4 ties together the ground observations measuring the end of the season and the mathematical detection of the start of the season. The validation was made based on 17 trees from the *M.excelsa* species which present regular and marked defoliation induced by the dry season. The extracted EVI signals showed an annual seasonal pattern although its temporality highly depends on the individual. For each of the 17 trees, the defoliation events appear regularly at each annual minimum EVI value or a bit subsequently. For the years 2017 and 2018, the observed defoliation was closely followed or even preceded by the SOS. Accounting for all the trees, the average differences between the observed defoliation and the SOS was 20.2 ± 25.2 in 2017 and 2.2 ± 8.9 in 2018.

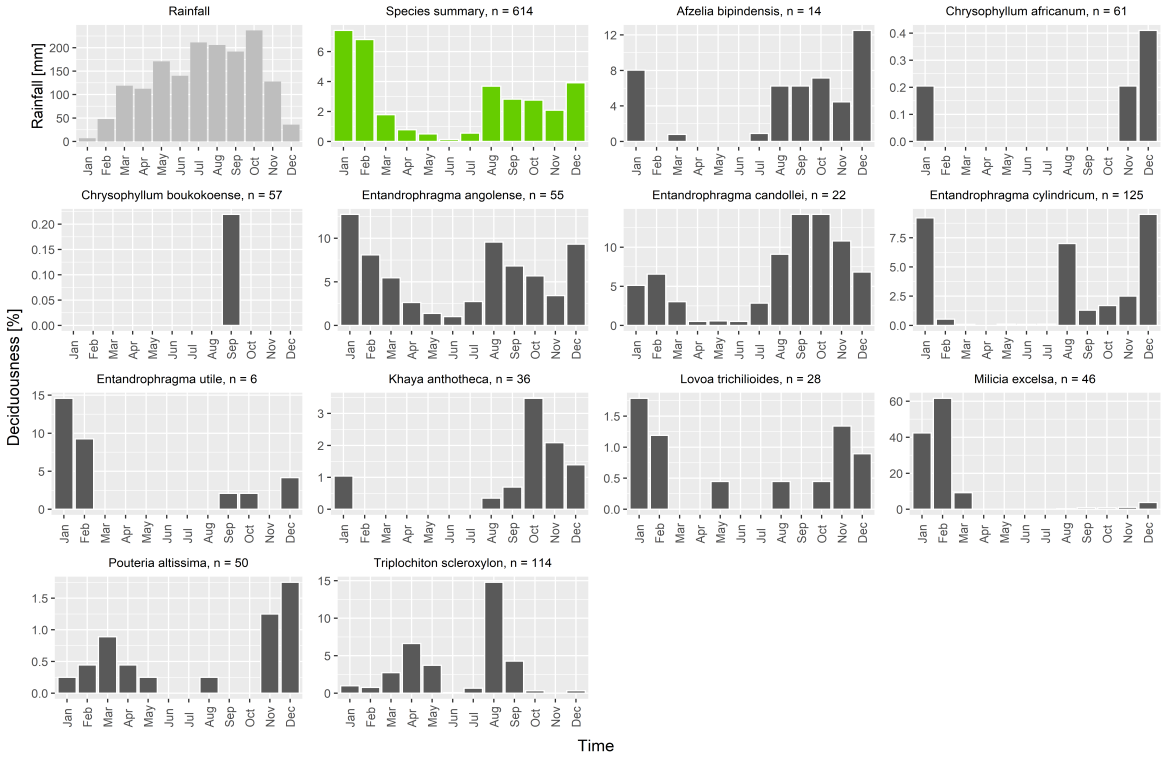

Figure 3.3: Monthly percentage of defoliated individuals (deciduousness) for each species (12) and accounting for all deciduous species (species summary) of the Mbaïki study site over the 2007-2013 and 2016-2018 periods. n represents the number of individuals. In parallel, the monthly rainfall (averaged over 2016-2020).

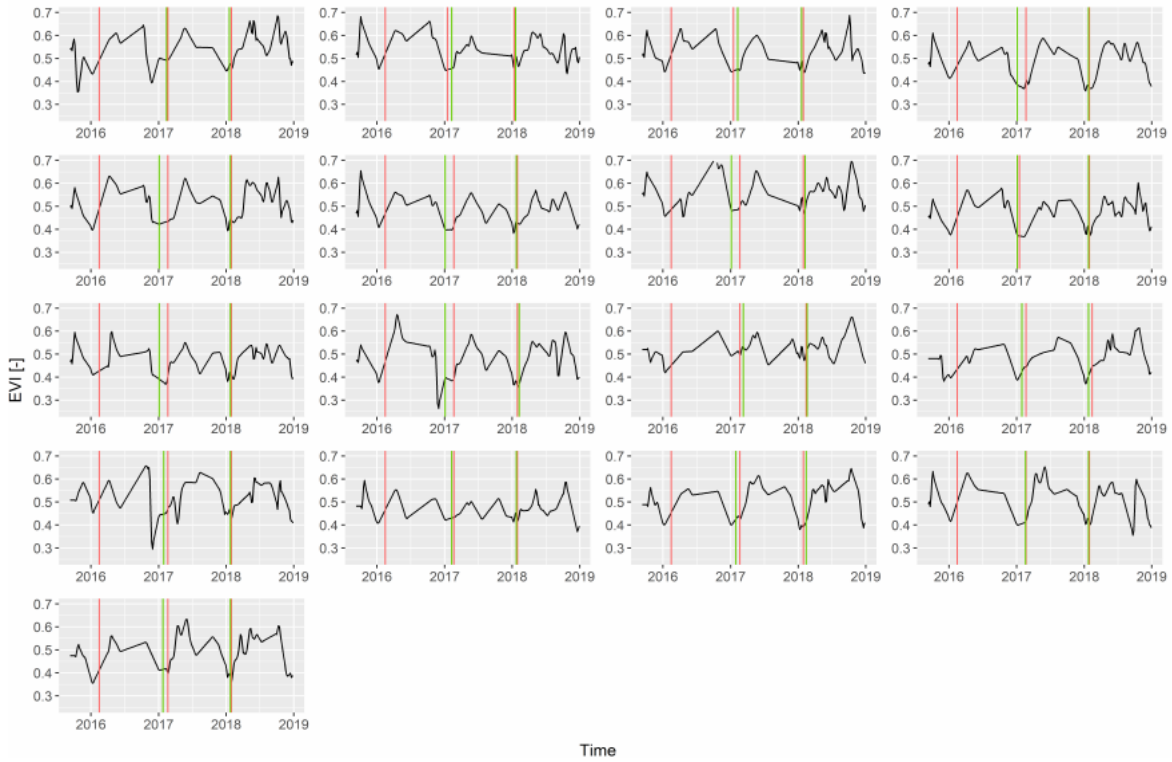

Figure 3.4: Savitsky-Golay smoothed EVI time series of 17 regularly defoliated trees of *M. excelsa*. The red vertical lines represent the ground observed defoliation for the period 2017 to 2019. The green vertical lines represent the Start Of the Season (SOS) for the years 2017 and 2018.

3.2.2 Vegetation dynamics

Globally, the four vegetation indices retrieved from Sentinel-2 images were able to capture the seasonal behaviour occurring in semi-deciduous forests and forest savannas and agricultural fields such as Mbaïki's (Appendix 6.1). Among all, the EVI was chosen for the remainder of this work because of its wide use in land surface phenology studies.

The seasonal dynamics of the EVI was presented in Figure 3.5 for the forest and non-forest pixels. Each land cover class accounted for a different number of pixels. The most represented land cover was the forest with 89.9% of the pixels. Each year, the two signals plummeted in the lowest rainfall months (grey bars in Figure 3.5). The rainfall time series revealed a regular annual rainfall pattern with, on average, the accumulated rainfall over the driest months (December to February) reaching 84.8 mm. However, the rainfall pattern was subject to interannual variations in intensity. The driest month was January commonly for each year although the dry period differs in the amount of rainfall accumulated. The year 2018 contained the driest month with 0 mm of accumulated rainfall. In contrast, the wettest month took place in October 2019 with 332 mm. Though, the wettest year of the time series was 2017 (total of 1803 mm). Regarding the EVI, the average amplitude, i.e. the difference between the seasonal maximum EVI and the seasonal minimum EVI, was equivalent to 0.32 $\pm$ 0.02 for the non-forest pixels. In the forest, the average amplitude was lower and reached the value of 0.21 $\pm$ 0.02. This higher amplitude in the non-forest compared to the forest

came from the systematically lower minimum and higher maximum encountered.

The patterns observed in Figure 3.5 were summarized annually in Figure 3.6. The lowest EVI value occurred at the end of the dry season (February) regardless of the land cover class, going from 0.39 (forest) to 0.35 (non-forest). The non-forest maximum EVI exceeded the forest with a value reaching 0.61 at the end of the wet season (October) against 0.57 for the forest in the middle of the wet season (May). While the rainfall seasonality was unimodal, two modes emerged in the vegetation dynamics with a secondary diminution in the EVI in the July to September period (Figure 3.6).

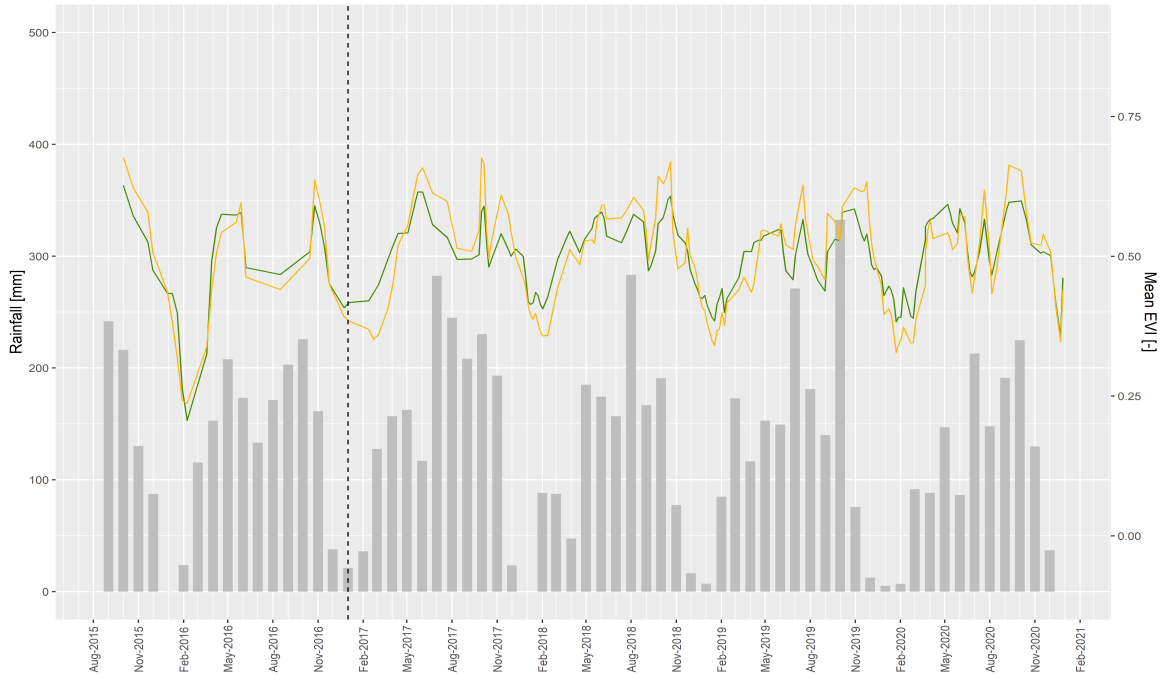

Figure 3.5: Savitsky-Golay smoothed time series of mean EVI (green and yellow lines) in parallel with the monthly rainfall time series (grey bars). Each index value was averaged over the study site (Mbaïki). In dark green, the forest class. In yellow, the non-forest class. The dotted black line mark the launch of the second Sentinel-2 satellite.

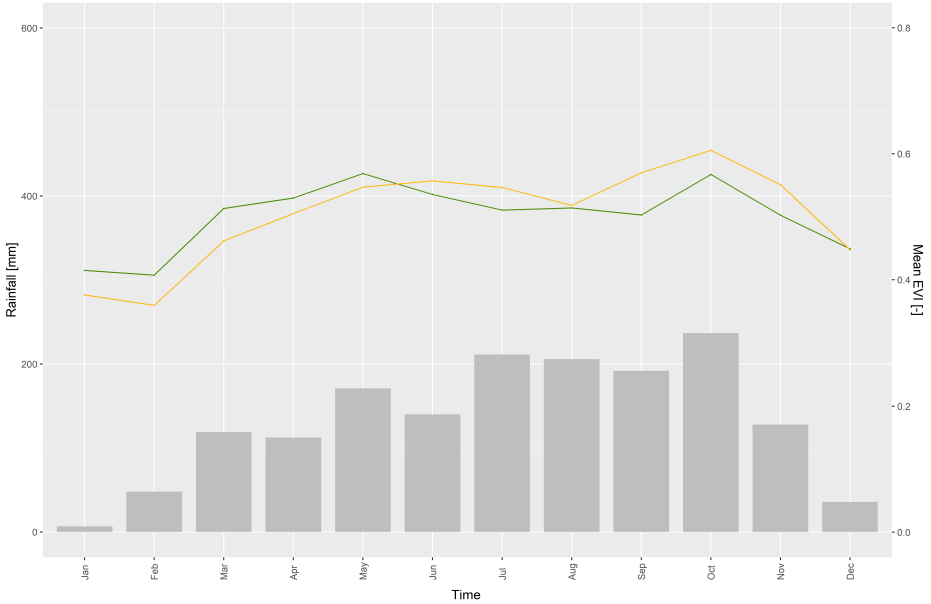

Figure 3.6: Synthetic year of the EVI for each land cover class. Each index value was monthly averaged over the study site (Mbaïki) and the study period (2015-2020). In dark green, the forest class. In yellow, the non-forest class. The bars are the monthly accumulated rainfall averaged yearly.

A deeper analysis of the seasonality in the Mbaïki site was made through a mathematical investigation: the wavelet transform. The interpretation of the continuous wavelet transform is based on the power coefficients to detect periodicity. The higher the power coefficient, the greater the similarity between the EVI signal and the signature of the parent wavelet (Morlet wavelet). The measured coefficients are given according to two components: time (x axis) and period (y axis). Therefore, the continuous wavelet transform indicates a given periodicity at a given time as a function of the value of the power coefficient. The cone of influence marks out the region in which the wavelets coefficient estimates are reliable.

The main resulting observation was the continuous yearly component appearing in both scalograms (Figure 3.7). Outside the cone of influence, the method was limited by the edge effect and the data should be interpreted carefully. However, given the continuous pattern occurring at the yearly scale, the annual frequency was considered as dominant for both forest and non forest. Nevertheless, the further ahead in the time series, the more the value of the coefficients faded, especially for the forest. After 2019, the forest coefficients were not significant anymore though still high. Regarding the non-forest pixels, the annual pattern was considered significant almost until the end of the time series (mid-2020). For both land cover classes, a semi-annual frequency was detected from mid-2018 for the forest class and from mid-2019 for the non-forest class, indicating the bimodality of the seasonal profile. The global power spectrum of the forest indicated another important frequency of 2 to 3 months matching yearly with the dry season timing. The non-forest seemed to undergo the same monthly recurrent events in the same years as the forest.

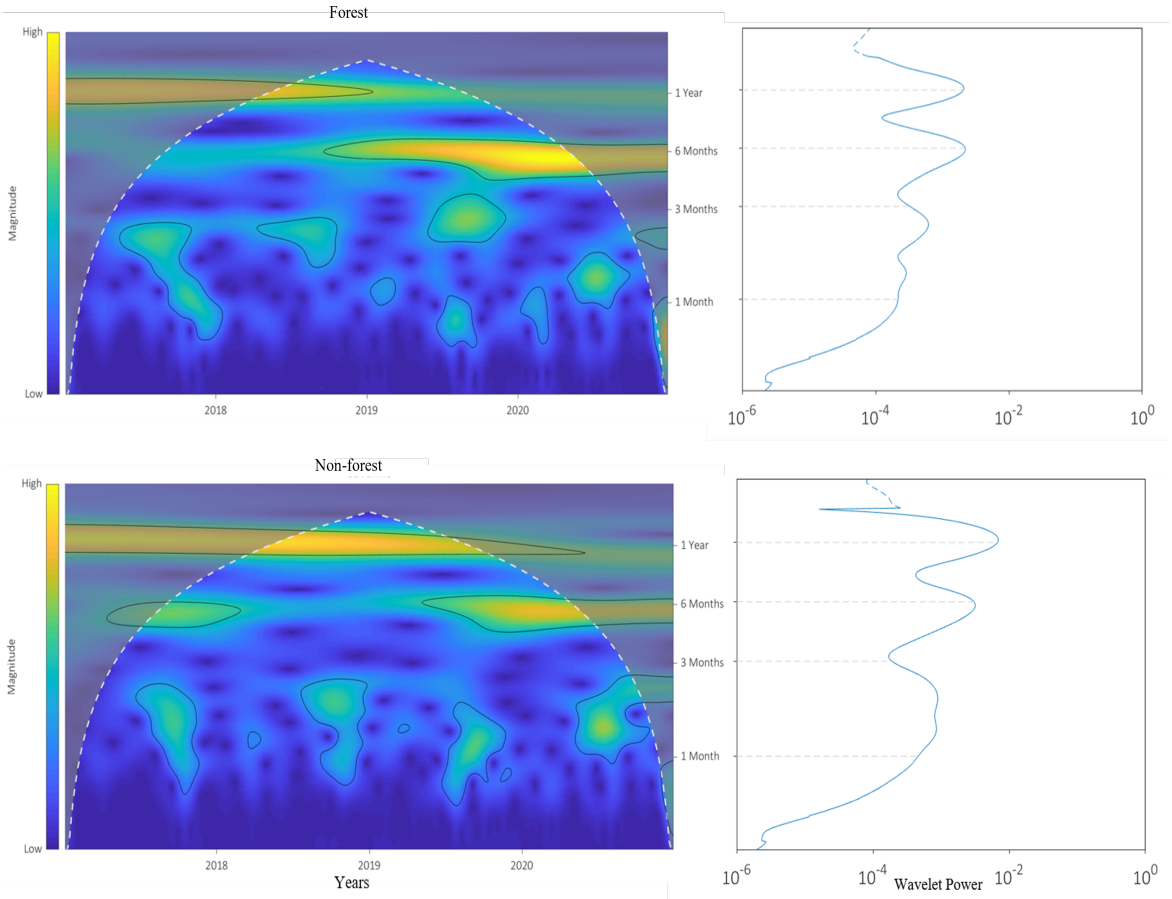

Figure 3.7: Power spectrum on the left and the global power spectrum on the right respectively for the forest and non-forest pixel EVI from 2017 to 2020 in Mbaïki. The shades from blue to yellow indicate the intensity of events, from low to high power coefficients. The significant coefficients are circled. The dotted line draws the limit of the cone of influence, i.e. non affected by the edge effects.

3.2.3 Rainfall influence

The influence of the rainfall on the vegetation greenness of Mbaïki was investigated based on the comparison between the Start Of the Season (SOS) and the Start Of Rain (SOR). The SOS matched in timing with the SOR season for both land cover (Appendix 6.2). For a given land cover class, the offset between the SOS and the SOR varied from one year to the next (Appendix 6.2, Table 3.1). The non-forest pixels tended to green up later than the forest pixels with respectively a mean day of year (doy) of 57.2 and 34.0 (February, Table 3.1). Moreover, on average, the non-forest greened up subsequently to the SOR while for the forest, the SOS is almost synchronized with the SOR. The earliest green-up occurred in 2019 (mean doy of 41.4, February) and matched with the earliest rain onset (doy of 20.0, January). The between years standard deviation of the SOS when considering both land covers was 4.9 against 12.7 for the SOR. Spatially, both land cover displayed between pixels variation around the same range from 16.4 (non-forest) to 18.7 (forest).

The spatial extent of the SOS and the associated histogram showing the frequency of the pixels for each SOS are presented in Figure 3.8. The pixels distribution was centred around the 20th (January) and 75th (March) doy for the 4 years. During the first year though, a second modality of lesser extent was observed from the 75th (March) and 100th (April) doy. Looking at the maps, each year, a group of orange-coloured pixels stands out testifying for a recurrent late green-up. Those pixels were found in the histogram from the 50th (February) to 100th (April) doy. The late green-up location matched with low tree cover percentage areas (Figure 2.3). The year 2019 attracts attention with an early SOR of 20 (January) compared to the other years. The pixels were greening synchronously and the distribution presents a main spike around the 24th (January) day, earlier than for the other years. Finally, the analysis of the in-between years spatial correlation of the green-up day revealed significant correlations going from 0.36 between 2018 and 2020 to 0.50 between 2017 and 2019.

Table 3.1: Yearly Start Of Rain (SOR) and Start Of the Season (SOS) expressed in day of year (doy) for each land cover class and for both in Mbaïki. The mean represents the averaged value over the 4 years. Spatial SD is the averaged spatial standard deviation (between pixels). Temporal SD is the temporal standard deviation (between years).

	2017	**2018**	**2019**	**2020**	**Mean**	**Spatial SD**	**Temporal SD**
SOR	41.8	36.0	20.0	50.0	37.0	1.6	12.7
SOS forest	39.0	34.2	27.3	35.5	34.0	18.7	4.9
SOS non-forest	65.6	54.7	53.1	55.4	57.2	16.4	5.7
SOS all	41.4	36.1	29.7	37.5	36.2	18.4	4.9

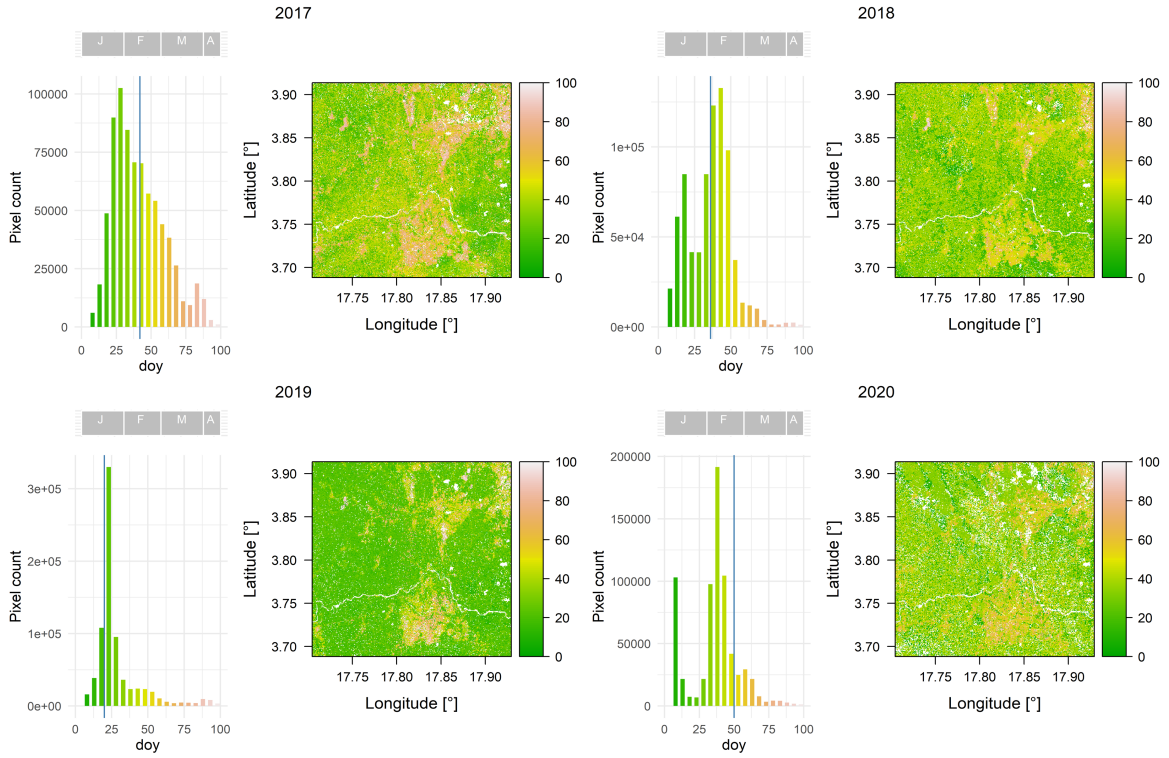

Figure 3.8: Yearly Start Of the Season (SOS) expressed in doy (day of year) over the 2017-2020 period represented on the left by a histogram and on the right by the spatial distribution. The green to orange colour palette highlights the timing of the SOS: early to late pixels. The vertical blue line sets the Start Of Rain (SOR). The grey bars express the corresponding month: January (J), February(F), March (M), April (A).

The wavelet coherence consists of a powerful tool to assess the correlation between the EVI signals and rainfall seasonality. The higher the correlation, the more signals evolve similarly and follow the same periodicity. In addition, the wavelet coherence provides information on the phase shifts between the two analysed signals (pinned by arrows in Figure 3.9). The results obtained for each of the land cover classes are presented in Figure 3.9. Focusing firstly on the yearly component, there was a high correlation between the forest and the rainfall signals as well as with the non-forest and the rainfall signals. The arrows pointing slightly to the upper right imply that the forest signal was ahead of the rain signal. The rainfall and non-forest signals were completely in phase. Regarding the semi-annual frequency, both the forest and the non-forest showed the same results: a high correlation between the rainfall and the EVI signals with the EVI that lags behind the rainfall. A final element can be drawn from the forest scalogram, a high correlation was detected at the 3 months period level from August 2018 to February 2020. The arrows stabilized as a phase between the forest and the rainfall signals. A similar phenomenon appeared in the non-forest coherence power spectrum from August 2018 to March 2019 but at the scale of 2 months. The non-forest was however late compared to the rainfall with a phase shift of approximately 1 month. The wavelet-coherence phase shifts resulted in an average advance of the forest of 16.9 $\pm$ 4.4 days. The non-forest areas showed an average delay of 1.9 $\pm$ 4.4 days for the 2017 - 2020 period.

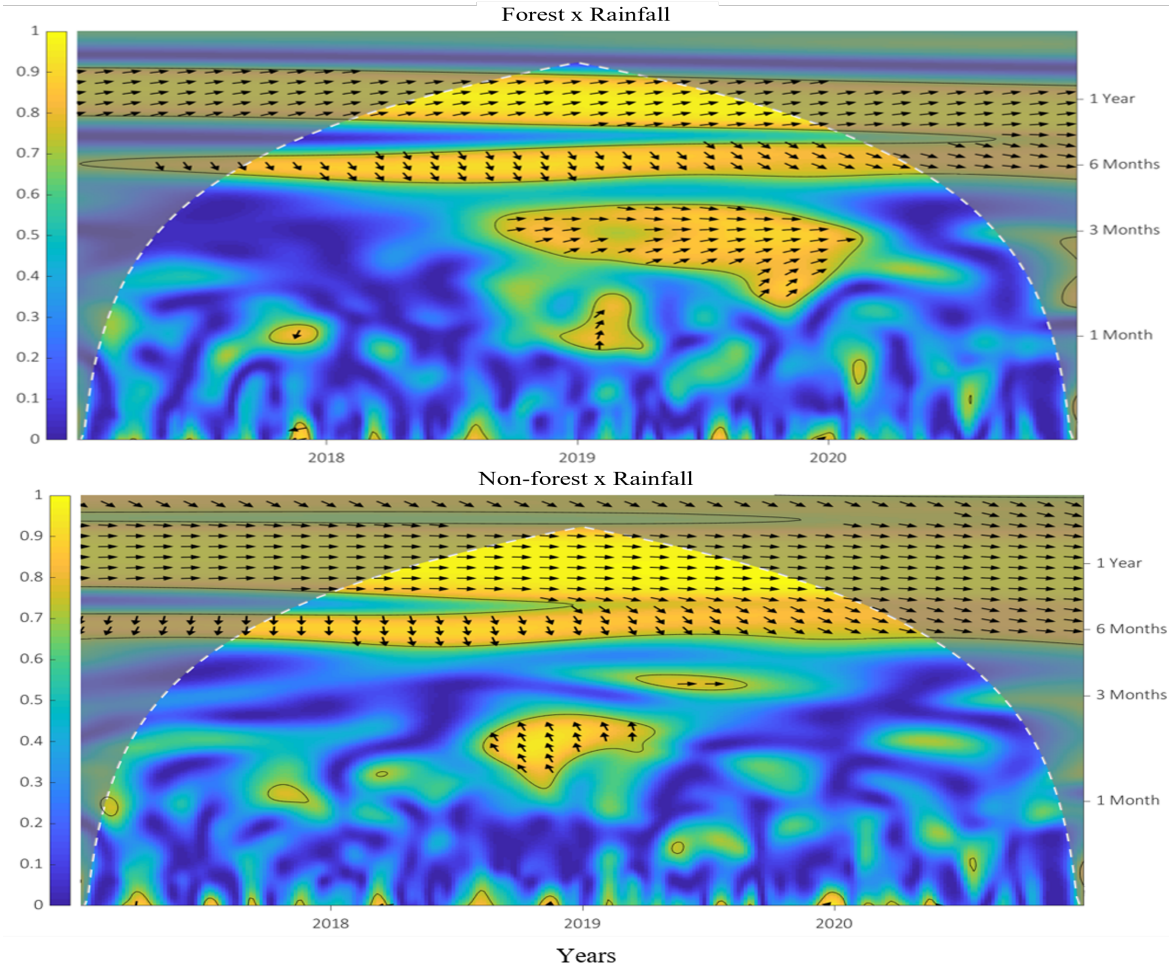

Figure 3.9: Wavelet coherence power spectrum (on the colour scale) and phase shift (arrows) between the forest and rainfall and the non-forest and rainfall. The blue (close to 0) indicates a low correlation while the yellow (close to 1) indicates a high correlation. An arrow pointing to the right specifies a phase match while an arrow to the left specifies a phase opposition. The correlations above 0.7 were circled.

3.3 Luki

In this section, the method was applied to a second study site located south of the equator in order to assess its potential for multi-site comparison.

3.3.1 Ground data

Figure 3.10 juxtaposes the rainfall and the ground observed deciduousness temporality over one average year. The main defoliation peaks were detected in September (9.40 %) and October (11.65 %), shifted toward the end of the dry season.

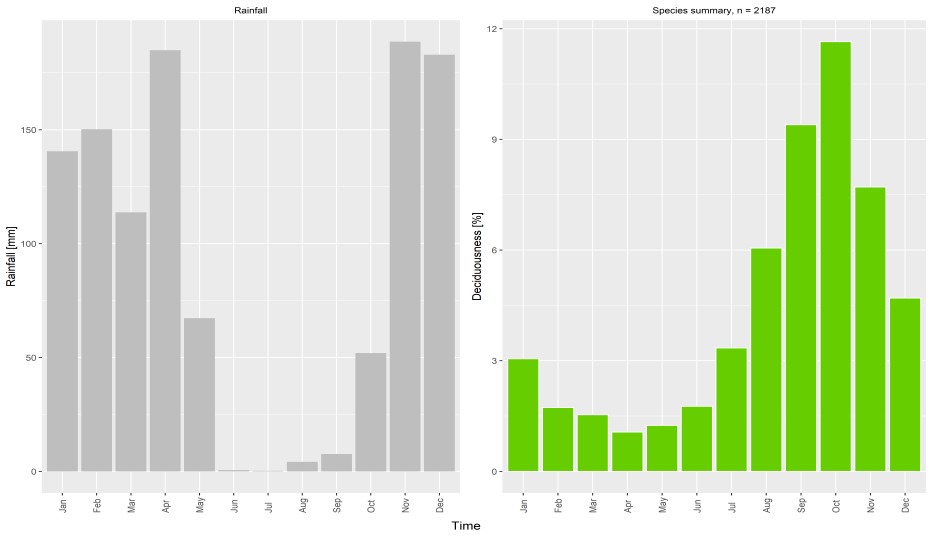

Figure 3.10: Monthly percentage of defoliated individuals (deciduousness) accounting for all deciduous species (species summary) of the Luki study site over the 1947-1958 period. n represents the number of individuals. In parallel, the monthly rainfall (averaged over 2016-2020).

3.3.2 Vegetation dynamics

As stated in Section 3.1.2, the Luki site was subject to high cloudiness and large data gaps were recurrent. Nevertheless, the time series displayed a seasonal behaviour although the low amount of data points produced unstable curves (Figure 3.11). A seasonal pattern could be observed in the EVI signals that bottomed out during the dry season (Figures 3.12). The lowest EVI values occurred for both land cover classes in August. On average, the minimum forest value was 0.41 and the minimum non-forest value was 0.38. In opposition, during the rainy season, the signals reached a maximum of 0.58 (forest) and 0.59 (non-forest). The rainfall seasonality was marked by a pronounced dry season. On average, from June to September, the accumulated rainfall reached 12.2 mm. Not a drop of water has fallen in July during the period of interest from 2017 to 2020 making it the driest month. In opposition, the wettest month occurred in November 2020 with 233 mm of accumulated rainfall whereas the wettest year was 2019 (1257 mm). Regarding the EVI time series (Figure 3.11), the forest and non-forest followed a similar yearly pattern. However, the non-forest reached lower minimum values but higher maximum values making its average amplitude of 0.27 $\pm$ 0.07 against 0.23 $\pm$ 0.06 for the forest.

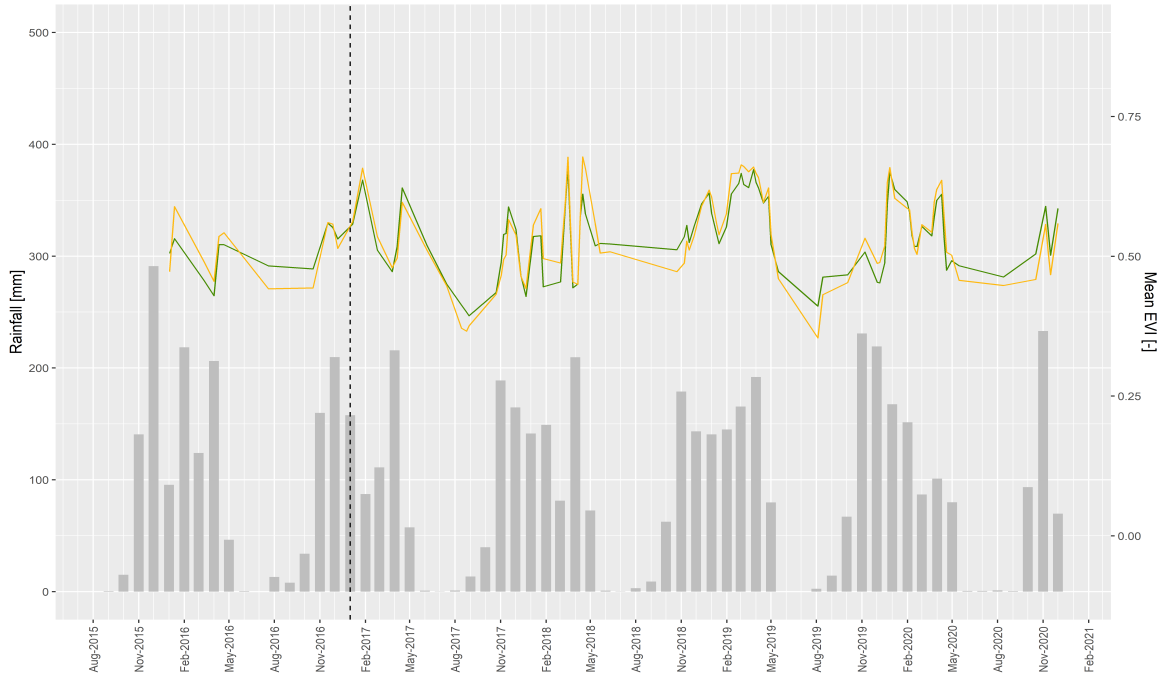

Figure 3.11: Savitsky-Golay smoothed time series of mean EVI (green and yellow lines) in parallel with the monthly rainfall time series (grey bars). Each index value was averaged over the study site (Luki). In dark green, the forest class. In yellow, the non-forest class. The dotted black line marks the launch of the second Sentinel-2 satellite.

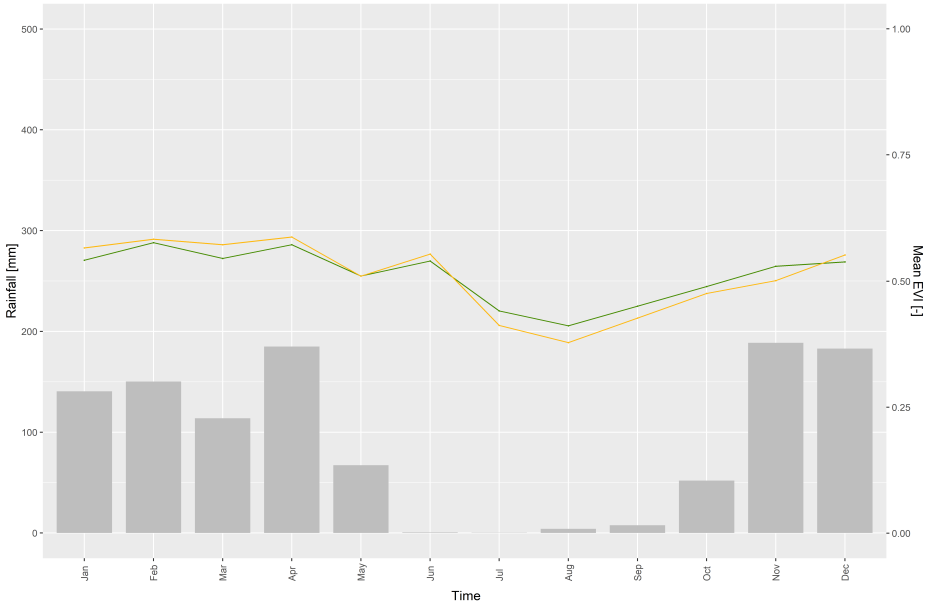

Figure 3.12: Synthetic year of the EVI for each land cover class. Each index value was monthly averaged over the study site (Luki) and the study period (2015-2020). In dark green, the forest class. In yellow, the non-forest class. The bars are the monthly accumulated rainfall averaged yearly.

3.3.3 Rainfall influence

Accordingly to the land cover class, there was a slight difference between the mean SOS of the forest greening approximately 1 day later than the non-forest (Table 3.2). However, it was not systematically the case with the greening of the non-forest in 2017 and 2018 later than the forest. On average and for both land cover classes, the SOS occurred before the SOR. In terms of spatial deviation, the non-forest and forest displayed analogous values around 30 days. Regarding the rainfall, the SOR was rather similar from one year to another except in 2019 for which the SOR of 266.5 (September) deviated the most from the average of 279.9 (October). In the same year, the corresponding SOS for both land cover classes showed the earliest green-up.

The three histogram distributions from 2017, 2019 and 2020 were bimodal (Figure 3.13) with a group of pixels greening up before the rainy season and another later. The year 2018 though only presented late green-up from the 280th (October) to 365th (December) doy. The earliest SOR occurring in 2019 was marked in the histogram (Figure 3.13) by the main spike of greening earlier compared to the other years. In 2017 and 2020 a notable number of pixels presented NA values, meaning that no green-up has been detected. This came from a lack of available images at the beginning and end of the time series. Finally, the analysis of the in-between years spatial correlation of the green-up day revealed significant correlations going from 0.02 between 2017 and 2018 to 0.20 between 2017 and 2020.

Nevertheless, for a considerable number of pixels, the large time lapse between two observations prevented the capture of the EVI minimum suspected to occur in the dry season. Therefore, when applying the same method as for Mbaïki, the green-up was rarely detected (NAs values in white on Figure 3.13). By taking two random pixels (Appendix 6.3), there was no trend of early or late green-up compared to the start of the rainy season. The timing between the SOS and SOR differed from one year to the next.

Table 3.2: Yearly Start Of Rain (SOR) and Start Of the Season (SOS) expressed in day of year (doy) for each land cover class and for both, in Luki. The mean represents the averaged value over the 4 years. Spatial SD is the averaged spatial standard deviation (between pixels). Temporal SD is the temporal standard deviation (between years).

	2017	**2018**	**2019**	**2020**	**Mean**	**Spatial SD**	**Temporal SD**
SOR	289.5	282.5	266.5	285.2	279.9	0.6	9.0
SOS forest	300.3	303.3	247.8	257.8	277.3	32.3	28.6
SOS non-forest	305.5	305.8	247.0	245.5	276.0	30.7	32.3
SOS all	301.3	303.8	247.6	254.7	276.9	32.0	29.8

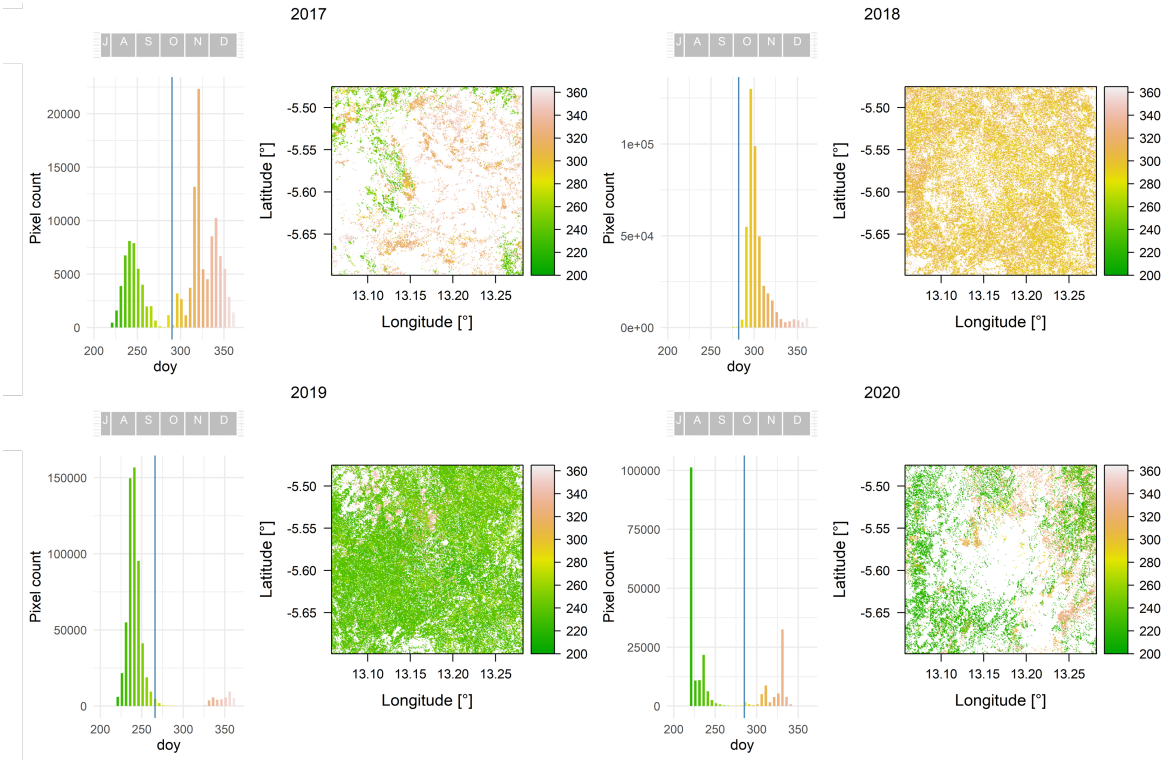

Figure 3.13: Yearly Start Of the Season (SOS) expressed in doy (day of year) over the 2017-2020 period represented on the left by a histogram and on the right by the spatial distribution. The green to orange colour palette highlights the timing of the SOS: early to late pixels. The vertical blue line sets the Start Of Rain (SOR).The grey bars express the corresponding month: July (J), August (A), September (S), October (O), November (N), December (D).

Chapter 4

Discussion and perspectives

This work demonstrated the suitability of Sentinel-2 data for phenology analyses in Central Africa despite the shortness of the time series. The discussion is divided into three main parts: the methodological approach (i), the vegetation seasonality (ii), and finally the rainfall control on phenology (iii).

4.1 Sentinel-2 data to monitor vegetation seasonality

4.1.1 Computational properties

The need was to produce a workflow that is easily applicable to multiple study sites. The challenge is met since the methodology that emerged has been applied to two study sites with a reverse seasonality due to northern (Mbaïki) and southern (Luki) influence. The combination of open access data sources including Sentinel-2 images and tree cover map from the Global Forest Watch open data portal (Hansen et al., 2013) allows the easy replication on multiple sites. Another significant advantage is its accessibility on standard desktop machines (typically i5 processor and 8 GB RAM) although dealing with Sentinel-2 data requires minimum disk space. In total, for one study site, the storage required reached 575.4 GB (Appendix 6.2). Comparatively to the *sen2R* toolbox from Ranghetti et al. (2020), the time requirement of the developed R codes used to perform the preprocessing steps was approximately two times higher (Appendix 6.1). The main limiting step is the atmospheric and topographic correction performed by the *sen2cor* algorithm developed by the ESA, followed by the retrieval of the start of the season and the start of rain (five hours and a half). In particular, the start of the season determination requires fulfilling a conditional statement for each measurement date and each pixels of the study area. This represents almost 700 000 pixels to process (30 m resolution, 25 x 25 km study area). The choice of 30 m resolution for start of the season extraction is justified by the reduction in time and RAM

required compared to the high computing power needed with 10 m resolution.

A point of interest for further work is to improve the codes' efficiency or use a more powerful machine to run in a lower amount of time in order to apply the method at a larger scale.

4.1.2 Method validation

The validation of the method was carried out by comparing ground data and satellite measurements and revealed the usability of the method outputs.

Firstly, the satellite metrics appeared to be sensitive to the main defoliation periods observed in the ground data collected in Mbaïki. The satellite signal is marked by a first decrease in greenness from December to February. The second wave of defoliation (August-September) is flagged by the signal but less intensively. These results support that Sentinel-2 satellites can capture the decrease in greenness further interpreted as leaf shedding. The validity of the Sentinel-2 EVI time series to retrieve phenological events such as leaf flushing and shedding has been previously assessed by Vrieling et al. (2018) by comparing the results from Sentinel-2 data and field cameras in a Dutch barrier island. In a validation study from Lange et al. (2017), Sentinel-2 leaf flush and leaf shed were found to be more consistent with ground-based sensor products than MODIS. Finally, the comparison of Sentinel-2 data with the PhenoCam metric in the Arctic tundra showed a high degree of similarity using the EVI as a vegetation index (Descals et al., 2020).

Secondly, the EVI has proven to be a successful indicator of greenness, as evidenced by its common use in land surface phenology studies (Adole et al., 2018; Moreira et al., 2019; Descals et al., 2020) from various satellite sensors (MODIS, Sentinel-2, etc.). However, the comparison between EVI values from different sensors must be done gingerly. The differences in hardware and software configuration from one sensor to another produces dissimilarities in the vegetation index values (Yoshioka et al., 2012). To limit this effect, the EVI definition is adapted depending on the sensor, in this case, suited for the Sentinel-2 sensors. Furthermore, even if only one sensor is considered, e.g. Sentinel-2, the characteristics of the location of interest may also influence the EVI values due to differences in atmospheric aerosol and soil brightness and colour (Xue and Su, 2017). This effect is however limited when using EVI that avoids the influence of the ground (Xue and Su, 2017).

Thirdly, the green-up day validation was made through the comparison of 17 monitored trees from *M.excelsa* to their corresponding EVI signal. The detected green-up occurred close to the measured defoliation. The simultaneity between these two processes, which at first sight seem antagonistic, actually reveals the validity of the green-up detection. Indeed, the ground measured defoliation is suspected to be shifted in time. First of all, the 15 days time interval between two observations may result in a delay in the leaf shedding detection.

This delay also comes from the ground definition of defoliation that is denoted when a field worker estimates the tree as totally defoliated. It is likely that when a tree is observed as defoliated from the ground, new leaves have already started to regrow on the top canopy. However, the spectral response evolves with leaves ageing (Roberts et al., 1998). The growth of young leaves causes a sudden rise in the EVI signal, detected as a green-up. In addition, although limited, two artefacts come into play. Firstly, the EVI signal is averaged over a 10m radius buffer around the georeferenced trees. It is likely that some of the averaged pixels are not part of the tree crown of interest and create noise such as evergreen trees or shrubs in the underlying canopy. Secondly, the accuracy of the georeferenced points is questionable.

Despite their ability to capture vegetation dynamics in Mbaïki, Sentinel-2's optical sensors may have some limitations that need to be taken into account when dealing with very dense canopies. In multi-layered forests, the understorey likely influences the reflectance measured by the satellite (Helman, 2018). Although the top canopy trees stand leafless, some of the understorey species may not be affected. This phenomenon is illustrated in Figure 4.1a, where the emergent trees are experiencing leaf loss and the underlying vegetation remains leafy. In addition, as reported by Helman (2018), the smoothing technique tends to erase the small variations in the signal. Especially in the case of very dense forests where the understorey layers buffer the changes in greenness in the top canopy. The complex multilayered system could hinder the Sentinel-2 satellite to capture low greenness variations that could represent some phenomena occurring in the canopy.

At last, in the present work, the use of the 70 % threshold to distinguish the forest from the non-forest, including mostly savanna but also rural complex around villages, is arbitrary. However, the savanna-forest distinction is vague in the literature and cannot rely on structural information only (Ratnam et al., 2011; Aleman et al., 2020). The lack of a clear definition of the tree savanna makes it difficult to compare with other studies. Figures 4.1a), b) and c) show the evolution from evergreen seasonal forest to tree savanna through transitional forest. The forest class is represented schematically by Figures a) and b). The non-forest is comparable to Figure 4.1c with a simpler structure and a continuous grass understorey (Ratnam et al., 2011).

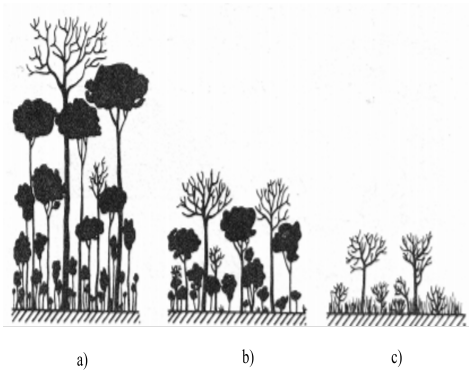

Figure 4.1: Schematic representation of a multi-layered canopy. a) Evergreen seasonal forest b) Transitional forest. c) Tree savanna. Figure taken from Longman and Jenìk (1974).

4.1.3 Cloud contamination: a major weakness

Owing to cloud interference, the time lag between two clear images can be substantial (up to 15.8 days in Luki). However, changes in leaf phenology occur rapidly (up to less than 15 days, Longman and Jenìk, 1974). Interpolation is therefore required to build continuous time series. In Luki, the persistent cloud cover masked a considerable number of pixels. A large amount of data gaps in the time series led to poor quality results. In fact, the western part of Central Africa is one of the most cloudy regions across the tropics (Philippon et al., 2019). The images quality obtain through optical remote sensors is lower than in other parts of Central Africa as reported by Gond et al. (2013). The limited accuracy may prevent the detection of the phenological response of the vegetation. In addition, undesirable effects appear from time to time in Sentinel-2 images leading to spatio-temporal inhomogeneity (Sudmanns et al., 2020). The higher the number of images, the less these noise-generating point effects will affect the results. This suggests that using Sentinel-2 as the unique data source is not enough when dealing with areas steadily contaminated by clouds.

The few authors using Sentinel-2 data recalled on complementary datasets to increase the number of observations. Kowalski et al. (2020) demonstrated that Sentinel-2 data alone are not sufficient in mountainous regions where the cloud cover is frequent and recognized the valuable use of Landsat-8 data to broaden the data acquisition. The revisit frequency goes from 5 days up to 3.5-4 days around the Equator from Sentinel-2 satellite only to combined Sentinel-2 and Landsat-8 data. Claverie et al. (2017) developed the Harmonized Landsat-Sentinel-2 (HLS) dataset that consists of consistent surface reflectance products derived from Sentinel-2 and Landsat 8 observations. Nowadays, HLS data are available over restricted areas of the world (mainly the USA) but were successfully used by several authors (Bolton et al., 2020; Griffiths et al., 2020). Another way to densify the land surface phenology time series is to use Synthetic Aperture Radar (SAR) images from Sentinel-1 coupled with Sentinel-2 data. On top of increasing the number of observations, SAR sensors are not tributary of cloudiness. At the present time, several studies investigated the potential benefit of combining those two datasets (Stendardi et al., 2019; d'Andrimont et al., 2020; Mercier et al., 2020; Meroni et al., 2021). Most revealed the relevance and complementarity of Sentinel-1 and -2 to monitor phenology. Combining these two datasets is not straightforward, as evidenced by the inability of Bush et al. (2020) to couple them when attempting to benefit from Sentinel-1 SAR and Sentinel-2 optical data in Gabon. An easily reproducible method is therefore needed for future research. To improve the interoperability of the here developed method, a solution is to incorporate Sentinel-1 to compensate for the lack of data. This combined use of Sentinel-2 and Sentinel-1 data would help to get rid of the cloud sensitivity from the optical sensors and increase the number of observations.

Finally, the last method adopted by scientists to increase temporal resolution and get rid of cloud cover problems is to use ground/canopy cameras, i.e. below the clouds (Nagai et al., 2016). These cameras, called Phenocams, take pictures automatically on a daily

basis. Phenocams are cost-effective and provide highly valuable continuous time series to monitor vegetation (Richardson et al., 2009;Alberton et al., 2017). For now, many studies benefited from the advantages of Phenocams in temperate forests, among others Richardson et al. (2009) in the USA and Wingate et al. (2015) in Europe. Vrieling et al. (2018) even combined Sentinel-2 and field cameras observations in a Dutch barrier. However, at present, images from digital cameras are still sparse in the tropics (Alberton et al., 2014; T. B. Brown et al., 2016). Lopes et al. (2016) though investigated the dry season green-up in central Amazon thanks to Phenocams. To undertake large scale studies in Central Africa, the Phenocams network needs to be extended.

4.2 Vegetation dynamics

The retrieval of the periodicity in the vegetation dynamics revealed the dominance of annual cycles both in Mbaïki and in Luki that vary in intensity depending on the land cover.

4.2.1 The annual pattern dominates

In both study sites, the EVI signal testifies for annual periodicity. The wavelet analysis further attests the dominance of annual cycles in vegetation functioning for the Mbaïki site. The preeminence of annual flowering and fruiting cycles has been previously demonstrated in Africa: in La Lopé National Park, Gabon (Bush et al., 2017), in a cross-site analysis (Adamescu et al., 2018), in Luki (Angoboy Ilondea et al., 2019) and using herbarium records (Ouédraogo et al., 2020).

As data became more available with the years, bi-annual patterns seem to emerge in the Mbaïki time series. Bi-modality has been earlier highlighted in the study area by regionalization of vegetation types based on seasonal functioning across the Sangha River interval using MODIS time-series (Gond et al., 2013, Figure 4.2). Philippon et al. (2019) extended this work by mapping forest types at the scale of Central Africa based on their EVI seasonality as well as the elevation, soils, ground data, and vegetation maps.

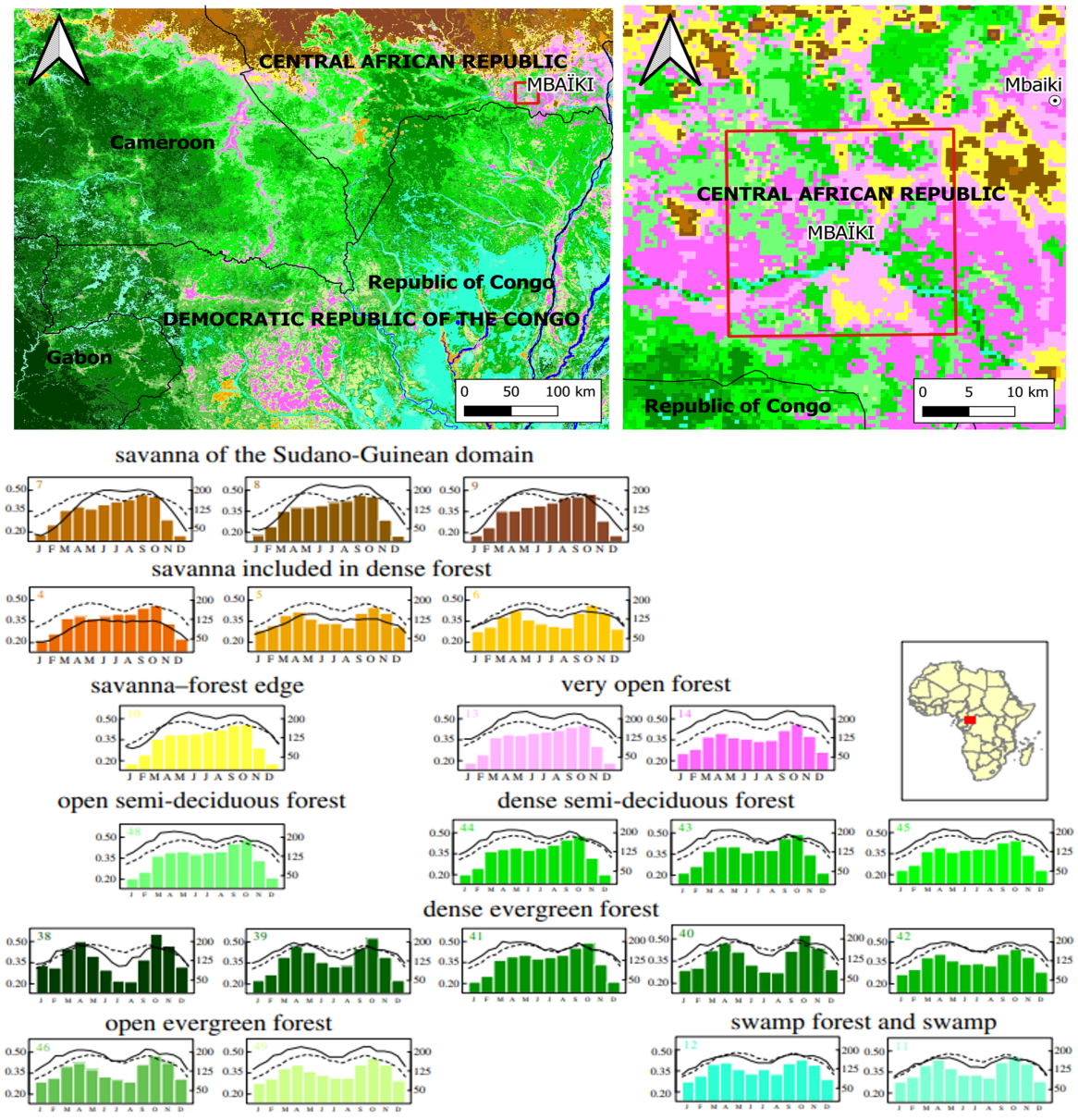

Figure 4.2: Vegetation map across the Sangha River interval. The mean EVI time series is shown for each vegetation class (solid line) as well as the mean time series over the entire study area (dashed line). Bars represent monthly rainfall. Figure taken from Gond et al. (2013).

4.2.2 Land cover influence

Distinct phenological behaviours separate the forest from the non-forest pixels. For instance, during the rainy season, the non-forest area is greener than the forest. Indeed, the tree crowns, consisting of old and new leaves, send a composite image of different spectral signatures and thus EVI values. In opposition, the areal part of herbaceous species greens up rather uniformly and sends a higher EVI signal.

In contrast, in the dry season, the forest is greener than the non-forest. A hypothesis comes from the complex multi-layered structure of the forest. It is suspected that the decline in the trees' greenness is compensated by the underlying vegetation but also by the appearance of new young leaves on the tree crown. In an ecosystem composed of fewer structural layers such as the non-forest (Figure 4.1a, b), the leaf shedding/yellowing leads to a drastic decrease in greenness.

A second hypothesis explaining the low minimum values of the non-forest is the practice of slash and burn agriculture (Longman and Jenìk, 1974). Especially in Mbaïki where the population is located close to the study region and the inhabitants regularly (once to two times a year) burn the wooded savannas and destroy the green part of the non-forest plants. The impact of these practices is largely dependant on the primary species composition. As discussed by Ratnam et al. (2011), the evolutionary and ecological traits considerably influence the differentiation between savanna and degraded forest. As far as the first class is concerned, the mix between trees and C4 grasses are adapted to recurrent fires and recover quickly. Regarding the degraded forest, fires are threatening the species equilibrium since the majority of species do not tolerate fires. In Mbaïki which is located at the northern edge of the margin of Congo Basin, the forest was progressively degraded and consists of a mix between savanna-forest and agriculture (Gond et al., 2013, Figure 4.2). To fully understand the mechanisms behind these dynamics, the parallel between the evolution of the vegetation index and the fire data would be valuable for further study.

4.3 Rainfall influence: ultimate or proximate cause

The relationship between rainfall and vegetation dynamics is underpinned in this work. The underlying is to distinguish the causality of rainfall that can exert a proximate or ultimate control. The analysis provided evidence to differentiate if the vegetation responds directly to rainfall or it is the result of long-term adaptation. This section will firstly relate the vegetation seasonality to the rainfall regime. Afterwards, arguments in favour ultimate and then proximate control of rainfall will be discussed.

4.3.1 Linking rainfall regime and vegetation seasonality

In Mbaïki, the wavelet coherence analysis links the vegetation cycle and the rainfall seasonality at the annual scale. In addition, the cross-site comparison confirmed a shift in the vegetation seasonality from Mbaïki to Luki in response to reverse rainfall regimes on both sides of the Equator (Ouédraogo et al., 2020). The timing of the leaf shedding events occurs in November-December in the northern hemisphere (Mbaïki) against Jun-Aug in the southern hemisphere (Luki). In contrast, on average, the green-up takes place around mid-February in the North and end-August in the South, at the beginning of the respective rainy season when the irradiance is high and the water available (Van Schaik et al., 1993). Rainfall has been demonstrated to play a key role in the leafing behaviours by many other studies (Reich and Borchert, 1984; M. E. Brown et al., 2010; Guan et al., 2015).

4.3.2 In favour of ultimate control of rainfall

In the first place, the between years comparison revealed that the start of rain displays a notably higher variability from one year to the next compared to the start of the season. This suggests that the principal factor triggering the leafing events is not directly the end of the dry season as it is argued by Ryan et al. (2017) and supports the ultimate control of rainfall.

This hypothesis is reinforced by the between years correlation. The significant correlation systematically observed in Mbaïki and Luki implies that the pixels undergoing late (early) green-up one year are subject to a late (early) green-up the next year. This supports a spatial factor driving the green-up. The late and early pixels are localized respectively over non-forested and forest pixels. In fact, in Mbaïki, the spatial pattern retrieved corresponds to the distinction in vegetation behaviour highlighted by Gond et al. (2013) over the study area (Figure 4.2). This involves a possible influence of the land cover on the green-up rather than the rainfall.

Furthermore, a trend of pre-rain green-up is observed in the MBaïki's forest: the forest signal evolved in advance compared to the rainfall and tends to exclude the proximate cause of rainfall. Across southern tropical Africa, the pre-rain green-up occurring in woodlands has been recently demonstrated by Ryan et al. (2017) and is due to the synergy between abiotic and biotic competition in temporal niche separation. However, it should not be forgotten that this non-simultaneity between the green-up and the start of rain may also be due to inaccuracies in the EVI, in particular, resulting from the gap-filling process.

Finally, in Mbaiki, the percentage of defoliation is important outside the dry season, implying defoliation unrelated to water shortage. This pattern potentially originates from genetic control. Many species have a large distribution in Central Africa, encompassing a

wide climatic spectrum. The two extremes on either side of the Equator present a single dry season, typically Mbaïki (North) and Luki (South). Nearby the Equator, the rainfall pattern is bimodal and two dry seasons occur. The multi-annual pattern observed in Mbaïki is decoupled from proximate cues and could be the result of the long evolutionary histories of species in this wide climatic space.

4.3.3 In favour of proximate control of rainfall

For both study sites, the earliest start of rain led to the earliest start of the season in 2019 supporting the hypothesis of rainfall as proximate factor rather than ultimate. Nevertheless, the 4 years long time series is limited to investigate with confidence the inter-annual variability. As soon as the Sentinel-2 time series grows in length, the investigation of the interannual variability could reveal key results to understand the processes driving the land surface phenology.

Furthermore, in opposition to the pre-rain green-up observed in the forest, the non-forest green-up takes place after the start of the rainy season and goes in favour of the proximate cause regarding the non-forest land cover. The antagonism between the early and late green-up respectively for the woody and herbaceous species has been recurrently observed (Sarmiento and Monasterio, 1983). In South Africa, Higgins et al. (2011) identified two distinct strategies from the forest and the savanna: respectively pre-rain and post-rain green-up. On average, in this work, the start of the season of the trees was 20 days before the savanna in Mbaïki against 10 days in South Africa (Higgins et al., 2011).

Lastly, if genetic control was the main factor triggering the start of the season, it would be expected that the spatial variation of the start of the season in the forest is higher than in the non-forest, given its higher Shannon diversity. However, the opposite pattern appears, the forest displayed a lower spatial variation than the non-forest. The same scenario was observed in South Africa where the lower the tree cover, the higher the spatial variability (Cho et al., 2017). They advanced the high dependence of grasses on water availability to link the high spatial variability of rainfall and high spatial variability in green-up. In this case, the low distortion in the rainfall does not allow to confirm this hypothesis. In fact, less competition in non-forest leading to less synchronized evolutionary traits could induce the difference. The implementation of a cross-site comparison is a powerful asset to confirm or inform the above-mentioned hypothesis but could not be met with the poor data quality of the Luki site.

4.4 Beyond rainfall

Rainfall is not the only driver of the leaf shedding and flushing events. In particular, in the case of Luki, the cloud cover alters the light availability and quality but also the atmospheric water demand (Philippon et al., 2019). The persistent cloud cover limits the atmospheric water demand and evapotranspiration enabling the trees to avoid water stress. Indeed, the dry season in Luki is more pronounced than in MBaiki with 84.8 mm in 3 months against 12.2 mm in 4 months. However, the minimal EVI values obtained in Mbaïki are lower than in Luki. Despite a strong water limitation in this period, a higher proportion of the vegetation in the Luki reserve remains green compared to the Mbaïki region. As argued in Gabon, the high level of cloud cover allows trees in the western part of Central Africa to maintain their leaves despite a low level of rainfall. Annual cumulative rainfall in Gabon is indeed below the 2000 mm threshold yr^{-1} recognised for maintaining photosynthetic activity (evergreen canopy) during the dry season in tropical forests worldwide (Guan et al., 2015). Luki evergreen trees appear to be an evolutionary trait to cope with the light-deficient climate.

Afterwards, an intriguing result is the peak of defoliation observed in August in Mbaïki's ground data that cannot be explained by the rainfall seasonality. These defoliation events can be associated with predation. Species such as *Triplochiton* and *Entandophragma* are particularly enjoyed by caterpillars. Indeed, lepidopter larvae at high enough population densities appear to be defoliators (Maisels, 2004). In the Mbaïki area, caterpillars are specifically appreciated by local populations and regularly collected during this season in the forest as non-wood forest products (Fayolle, pers. com.).

Finally, the influence of other environmental factors besides rainfall may explain the reverse vegetation seasonality that does not perfectly match the reverse rainfall seasonality in tropical African forests (Ouédraogo et al., 2020). In fact, Ouédraogo et al. (2020) demonstrated reverse seasonality but outside the forest, in the savanna area, where the rainfall control might be more important.

Chapter 5

Conclusion

Through the development of a workflow, this work has enabled the use of the recently available Sentinel-2 datasets and proves its ability to monitor the seasonality of vegetation over Central Africa as long as cloud contamination remains reasonable. As observed repeatedly over the tropics, cloud cover is the main problem when it comes to optical sensors. This study highlighted the need for coupling data sources to cope with cloud contamination.

By this work, the dominance of annual cycles in the leafing pattern is confirmed and a bi-annual pattern is detected. Bi-annual cycles need to be further investigated as soon as the Sentinel-2 time series covers a longer period. Depending on the land cover, the phenological behaviors diverge in terms of minimum and maximum annual values although annual cycles are observed in both.

Furthermore, the relationship between rainfall and vegetation dynamics is emphasized. Arguments were advanced both in favor of ultimate and proximate cause that exacerbates the requirement of extensive research to decouple the two causes. Nonetheless, the observed forest cover pre-rain green-up is in line with the ultimate control previously suspected in the literature.

Implementing this method at a regional scale in parallel with multiple environmental variables (rainfall, irradiance, soil properties) would provide a deeper understanding of the environmental cues driving the leaf shedding and flushing events in Central Africa.

Bibliography

Abernethy, K., Bush, E. R., Forget, P.-M., Mendoza, I., & Morellato, L. P. C. (2018). Current issues in tropical phenology: A synthesis. *Biotropica*, *50*(3), 477–482.

Achard, F., Beuchle, R., Mayaux, P., Stibig, H.-J., Bodart, C., Brink, A., Carboni, S., Desclée, B., Donnay, F., Eva, H. D., et al. (2014). Determination of tropical deforestation rates and related carbon losses from 1990 to 2010. *Global change biology*, *20*(8), 2540–2554.

Adamescu, G. S., Plumptre, A. J., Abernethy, K. A., Polansky, L., Bush, E. R., Chapman, C. A., Shoo, L. P., Fayolle, A., Janmaat, K. R., Robbins, M. M., et al. (2018). Annual cycles are the most common reproductive strategy in african tropical tree communities. *Biotropica*, *50*(3), 418–430.

Adole, T., Dash, J., & Atkinson, P. M. (2016). A systematic review of vegetation phenology in africa. *Ecological Informatics*, *34*, 117–128.

Adole, T., Dash, J., & Atkinson, P. M. (2018). Characterising the land surface phenology of africa using 500 m modis evi. *Applied geography*, *90*, 187–199.

Alberton, B., Almeida, J., Helm, R., Torres, R. d. S., Menzel, A., & Morellato, L. P. C. (2014). Using phenological cameras to track the green up in a cerrado savanna and its on-the-ground validation. *Ecological Informatics*, *19*, 62–70.

Alberton, B., Torres, R. d. S., Cancian, L. F., Borges, B. D., Almeida, J., Mariano, G. C., dos Santos, J., & Morellato, L. P. C. (2017). Introducing digital cameras to monitor plant phenology in the tropics: Applications for conservation. *Perspectives in Ecology and Conservation*, *15*(2), 82–90.

Aleman, J., Fayolle, A., Favier, C., Staver, A. C., Dexter, K. G., Ryan, C., Azihou, A. F., Bauman, D., te Beest, M., Chidumayo, E. N., et al. (2020). Floristic evidence for alternative biome states in tropical africa. *Proceedings of the National Academy of Sciences*, *117*(45), 28183–28190.

Angoboy Ilondea, B., Beeckman, H., Ouedraogo, D.-Y. O., Bourland, N., De Mil, T., Van Den Bulcke, J., Van Acker, J., Couralet, C., Ewango, C., Hubau, W., et al. (2019). Une forte saisonnalité du climat et de la phénologie reproductive dans la forêt du mayombe: L'apport des données historiques de la réserve de luki en république démocratique du congo. *BOIS & FORETS DES TROPIQUES*, *341*, 39–53.

Archibald, S., & Scholes, R. (2007). Leaf green-up in a semi-arid african savanna-separating tree and grass responses to environmental cues. *Journal of Vegetation Science*, *18*(4), 583–594.

Asner, G. P. (2001). Cloud cover in landsat observations of the brazilian amazon. *International journal of remote sensing*, *22*(18), 3855–3862.

Asner, G. P., Townsend, A. R., & Braswell, B. H. (2000). Satellite observation of el nino effects on amazon forest phenology and productivity. *Geophysical research letters*, *27*(7), 981–984.

Azzali, S., & Menenti, M. (2000). Mapping vegetation-soil-climate complexes in southern africa using temporal fourier analysis of noaa-avhrr ndvi data. *International Journal of Remote Sensing*, *21*(5), 973–996.

Ben Abbes, A., Bounouh, O., Farah, I. R., de Jong, R., & Martínez, B. (2018). Comparative study of three satellite image time-series decomposition methods for vegetation change detection. *European Journal of Remote Sensing*, *51*(1), 607–615.

Bolton, D. K., Gray, J. M., Melaas, E. K., Moon, M., Eklundh, L., & Friedl, M. A. (2020). Continental-scale land surface phenology from harmonized landsat 8 and sentinel-2 imagery. *Remote Sensing of Environment*, *240*, 111685.

Bouvet, A., Mermoz, S., Le Toan, T., Villard, L., Mathieu, R., Naidoo, L., & Asner, G. P. (2018). An above-ground biomass map of african savannahs and woodlands at 25 m resolution derived from alos palsar. *Remote sensing of environment*, *206*, 156–173.

Brown, M. E., de Beurs, K., & Vrieling, A. (2010). The response of african land surface phenology to large scale climate oscillations. *Remote Sensing of Environment*, *114*(10), 2286–2296.

Brown, T. B., Hultine, K. R., Steltzer, H., Denny, E. G., Denslow, M. W., Granados, J., Henderson, S., Moore, D., Nagai, S., SanClements, M., et al. (2016). Using phenocams to monitor our changing earth: Toward a global phenocam network. *Frontiers in Ecology and the Environment*, *14*(2), 84–93.

Bush, E. R., Abernethy, K. A., Jeffery, K., Tutin, C., White, L., Dimoto, E., Dikangadissi, J.-T., Jump, A. S., & Bunnefeld, N. (2017). Fourier analysis to detect phenological cycles using long-term tropical field data and simulations. *Methods in Ecology and Evolution*, *8*(5), 530–540.

Bush, E. R., Mitchard, E. T., Silva, T. S., Dimoto, E., Dimbonda, P., Makaga, L., & Abernethy, K. (2020). Monitoring mega-crown leaf turnover from space. *Remote Sensing*, *12*(3), 429.

Cai, Y., Li, X., Zhang, M., & Lin, H. (2020). Mapping wetland using the object-based stacked generalization method based on multi-temporal optical and sar data. *International Journal of Applied Earth Observation and Geoinformation*, *92*, 102164.

Camberlin, P., Barraud, G., Bigot, S., Dewitte, O., Makanzu Imwangana, F., Maki Mateso, J.-C., Martiny, N., Monsieurs, E., Moron, V., Pellarin, T., et al. (2019). Evaluation of remotely sensed rainfall products over central africa. *Quarterly Journal of the Royal Meteorological Society*, *145*(722), 2115–2138.

Ceballos, G., Ehrlich, P. R., Barnosky, A. D., García, A., Pringle, R. M., & Palmer, T. M. (2015). Accelerated modern human–induced species losses: Entering the sixth mass extinction. *Science advances*, *1*(5), e1400253.

Cho, M. A., Ramoelo, A., & Dziba, L. (2017). Response of land surface phenology to variation in tree cover during green-up and senescence periods in the semi-arid savanna of southern africa. *Remote Sensing*, *9*(7), 689.

Claverie, M., Masek, J. G., Ju, J., & Dungan, J. L. (2017). Harmonized landsat-8 sentinel-2 (hls) product user's guide. *National Aeronautics and Space Administration (NASA): Washington, DC, USA*.

Cleland, E. E., Chuine, I., Menzel, A., Mooney, H. A., & Schwartz, M. D. (2007). Shifting plant phenology in response to global change. *Trends in ecology & evolution*, *22*(7), 357–365.

d'Andrimont, R., Taymans, M., Lemoine, G., Ceglar, A., Yordanov, M., & van der Velde, M. (2020). Detecting flowering phenology in oil seed rape parcels with sentinel-1 and-2 time series. *Remote sensing of environment*, *239*, 111660.

Descals, A., Verger, A., Yin, G., & Peñuelas, J. (2020). Improved estimates of arctic land surface phenology using sentinel-2 time series. *Remote Sensing*, *12*(22), 3738.

Dezfuli, A. K., Ichoku, C. M., Huffman, G. J., Mohr, K. I., Selker, J. S., Van De Giesen, N., Hochreutener, R., & Annor, F. O. (2017). Validation of imerg precipitation in africa. *Journal of hydrometeorology*, *18*(10), 2817–2825.

ESA. (2015a). *Sentinel-2 user handbook*. European Space Agency.

ESA. (2015b). The story of sentinel-2. *European Space Agency Bulletin*, *161*, 8.

ESA. (2018). *Sen2cor configuration and user manual*. European Space Agency.

Féret, J.-B., & de Boissieu, F. (2020). Biodivmapr: An r package for α-and β-diversity mapping using remotely sensed images. *Methods in Ecology and Evolution*, *11*(1), 64–70.

Fu, Y. H., Zhao, H., Piao, S., Peaucelle, M., Peng, S., Zhou, G., Ciais, P., Huang, M., Menzel, A., Peñuelas, J., et al. (2015). Declining global warming effects on the phenology of spring leaf unfolding. *Nature*, *526*(7571), 104–107.

GEO BON. (2017). Geo bon implementation plan 2017–2020 (version 1.3).

Gond, V., Fayolle, A., Pennec, A., Cornu, G., Mayaux, P., Camberlin, P., Doumenge, C., Fauvet, N., & Gourlet-Fleury, S. (2013). Vegetation structure and greenness in central africa from modis multi-

temporal data. *Philosophical Transactions of the Royal Society B: Biological Sciences*, *368*(1625), 20120309.

Gourlet-Fleury, S., Beina, D., Fayolle, A., Ouédraogo, D.-Y., Mortier, F., Bénédet, F., Closset-Kopp, D., & Decocq, G. (2013). Silvicultural disturbance has little impact on tree species diversity in a central african moist forest. *Forest Ecology and Management*, *304*, 322–332.

Grabska, E., Hostert, P., Pflugmacher, D., & Ostapowicz, K. (2019). Forest stand species mapping using the sentinel-2 time series. *Remote Sensing*, *11*(10), 1197.

Granero-Belinchon, C., Adeline, K., Lemonsu, A., & Briottet, X. (2020). Phenological dynamics characterization of alignment trees with sentinel-2 imagery: A vegetation indices time series reconstruction methodology adapted to urban areas. *Remote Sensing*, *12*(4), 639.

Griffiths, P., Nendel, C., Pickert, J., & Hostert, P. (2020). Towards national-scale characterization of grassland use intensity from integrated sentinel-2 and landsat time series. *Remote Sensing of Environment*, *238*, 111124.

Guan, K., Pan, M., Li, H., Wolf, A., Wu, J., Medvigy, D., Caylor, K. K., Sheffield, J., Wood, E. F., Malhi, Y., et al. (2015). Photosynthetic seasonality of global tropical forests constrained by hydroclimate. *Nature Geoscience*, *8*(4), 284–289.

Hansen, M. C., Potapov, P. V., Moore, R., Hancher, M., Turubanova, S. A., Tyukavina, A., Thau, D., Stehman, S., Goetz, S. J., Loveland, T. R., et al. (2013). High-resolution global maps of 21st-century forest cover change. *science*, *342*(6160), 850–853.

Helman, D. (2018). Land surface phenology: What do we really 'see'from space? *Science of the Total Environment*, *618*, 665–673.

Henebry, G. M., & de Beurs, K. M. (2013). Remote sensing of land surface phenology: A prospectus. *Phenology: An integrative environmental science* (pp. 385–411). Springer.

Higgins, S. I., Delgado-Cartay, M. D., February, E. C., & Combrink, H. J. (2011). Is there a temporal niche separation in the leaf phenology of savanna trees and grasses? *Journal of Biogeography*, *38*(11), 2165–2175.

Hou, A. Y., Kakar, R. K., Neeck, S., Azarbarzin, A. A., Kummerow, C. D., Kojima, M., Oki, R., Nakamura, K., & Iguchi, T. (2014). The global precipitation measurement mission. *Bulletin of the American Meteorological Society*, *95*(5), 701–722.

Huete, A., Didan, K., Shimabukuro, Y. E., Ratana, P., Saleska, S. R., Hutyra, L. R., Yang, W., Nemani, R. R., & Myneni, R. (2006). Amazon rainforests green-up with sunlight in dry season. *Geophysical research letters*, *33*(6).

Huete, A., Restrepo-Coupe, N., Ratana, P., Didan, K., Saleska, S., Ichii, K., Panuthai, S., & Gamo, M. (2008). Multiple site tower flux and remote sensing comparisons of tropical forest dynamics in monsoon asia. *Agricultural and Forest Meteorology*, *148*(5), 748–760.

Huete, A., & Saleska, S. (2010). Remote sensing of tropical forest phenology: Issues and controversies. *Int. Arch. Photogammetry Remote Sens. Spat. Inf. Sci*, *38*(8).

Huffman, G. J., Bolvin, D. T., Braithwaite, D., Hsu, K., Joyce, R., Xie, P., & Yoo, S.-H. (2020). Nasa global precipitation measurement (gpm) integrated multi-satellite retrievals for gpm (imerg). *Algorithm Theoretical Basis Document (ATBD) Version*, *6*, 31.

Huffman, G., Stocker, E., Bolvin, D., Nelkin, E., & Tan, J. (2019). Gpm imerg final precipitation l3 1 day 0.1 degree x 0.1 degree v06 (edited by andrey savtchenko, greenbelt, md, goddard earth sciences data and information services center (ges disc)). *doi. org/10.5067/GPM/IMERG DF/DAY/06*.

Jönsson, P., Cai, Z., Melaas, E., Friedl, M. A., & Eklundh, L. (2018). A method for robust estimation of vegetation seasonality from landsat and sentinel-2 time series data. *Remote Sensing*, *10*(4), 635.

Kowalski, K., Senf, C., Hostert, P., & Pflugmacher, D. (2020). Characterizing spring phenology of temperate broadleaf forests using landsat and sentinel-2 time series. *International Journal of Applied Earth Observation and Geoinformation*, *92*, 102172.

Lange, M., Dechant, B., Rebmann, C., Vohland, M., Cuntz, M., & Doktor, D. (2017). Validating modis and sentinel-2 ndvi products at a temperate deciduous forest site using two independent ground-based sensors. *Sensors*, *17*(8), 1855.

Lewis, S. L., Edwards, D. P., & Galbraith, D. (2015). Increasing human dominance of tropical forests. *Science*, *349*(6250), 827–832.

Liu, L., Xiao, X., Qin, Y., Wang, J., Xu, X., Hu, Y., & Qiao, Z. (2020). Mapping cropping intensity in china using time series landsat and sentinel-2 images and google earth engine. *Remote Sensing of Environment*, *239*, 111624.

Longman, K. A., & Jenìk, J. (1974). *Tropical forest and its environment*. Longman Group Ltd.

Lopes, A. P., Nelson, B. W., Wu, J., de Alencastro Graça, P. M. L., Tavares, J. V., Prohaska, N., Martins, G. A., & Saleska, S. R. (2016). Leaf flush drives dry season green-up of the central amazon. *Remote Sensing of Environment*, *182*, 90–98.

Lubini, A. (1997). *La végétation de la réserve de biosphère de luki au mayombe (zaïre)* (Vol. 10). Jardin botanique national de Belgique.

Mahdianpari, M., Salehi, B., Mohammadimanesh, F., Homayouni, S., & Gill, E. (2019). The first wetland inventory map of newfoundland at a spatial resolution of 10 m using sentinel-1 and sentinel-2 data on the google earth engine cloud computing platform. *Remote Sensing*, *11*(1), 43.

Maisels, F. (2004). Defoliation of a monodominant rain-forest tree by a noctuid moth in gabon. *Journal of tropical ecology*, *20*(2), 239–241.

Malhi, Y., Gardner, T. A., Goldsmith, G. R., Silman, M. R., & Zelazowski, P. (2014). Tropical forests in the anthropocene. *Annual Review of Environment and Resources*, *39*, 125–159.

Martinez, B., & Gilabert, M. A. (2009). Vegetation dynamics from ndvi time series analysis using the wavelet transform. *Remote sensing of environment*, *113*(9), 1823–1842.

Menaut, J.-C., Lepage, M., & Abbadie, L. (1995). Savannas, woodlands and dry forests in africa. In S. H. Bullock, H. A. Mooney, & E. Medina (Eds.), *Seasonally dry tropical forests* (pp. 64–92). Cambridge University Press. https://doi.org/10.1017/CBO9780511753398.004

Menzel, A., & Fabian, P. (1999). Growing season extended in europe. *Nature*, *397*(6721), 659–659.

Mercier, A., Betbeder, J., Baudry, J., Le Roux, V., Spicher, F., Lacoux, J., Roger, D., & Hubert-Moy, L. (2020). Evaluation of sentinel-1 & 2 time series for predicting wheat and rapeseed phenological stages. *ISPRS Journal of Photogrammetry and Remote Sensing*, *163*, 231–256.

Meroni, M., d'Andrimont, R., Vrieling, A., Fasbender, D., Lemoine, G., Rembold, F., Seguini, L., & Verhegghen, A. (2021). Comparing land surface phenology of major european crops as derived from sar and multispectral data of sentinel-1 and-2. *Remote sensing of environment*, *253*, 112232.

Misra, G., Cawkwell, F., & Wingler, A. (2020). Status of phenological research using sentinel-2 data: A review. *Remote Sensing*, *12*(17), 2760.

Moreira, A., Fontana, D. C., & Kuplich, T. M. (2019). Wavelet approach applied to evi/modis time series and meteorological data. *ISPRS journal of photogrammetry and remote sensing*, *147*, 335–344.

Morton, D. C., Nagol, J., Carabajal, C. C., Rosette, J., Palace, M., Cook, B. D., Vermote, E. F., Harding, D. J., & North, P. R. (2014). Amazon forests maintain consistent canopy structure and greenness during the dry season. *Nature*, *506*(7487), 221–224.

Myers, N. (1996). The world's forests: Problems and potentials. *Environmental Conservation*, 156–168.

Nagai, S., Ichie, T., Yoneyama, A., Kobayashi, H., Inoue, T., Ishii, R., Suzuki, R., & Itioka, T. (2016). Usability of time-lapse digital camera images to detect characteristics of tree phenology in a tropical rainforest. *Ecological Informatics*, *32*, 91–106.

Newstrom, L. E., Frankie, G. W., & Baker, H. G. (1994). A new classification for plant phenology based on flowering patterns in lowland tropical rain forest trees at la selva, costa rica. *Biotropica*, 141–159.

Ouédraogo, D.-Y., Fayolle, A., Gourlet-Fleury, S., Mortier, F., Freycon, V., Fauvet, N., Rabaud, S., Cornu, G., Bénédet, F., Gillet, J.-F., et al. (2016). The determinants of tropical forest deciduousness: Disentangling the effects of rainfall and geology in central africa. *Journal of Ecology*, *104*(4), 924–935.

Ouédraogo, D.-Y., Hardy, O. J., Doucet, J.-L., Janssens, S. B., Wieringa, J. J., Stoffelen, P., Ilondea, B. A., Baya, F., Beeckman, H., Daïnou, K., et al. (2020). Latitudinal shift in the timing of flowering of tree species across tropical africa: Insights from field observations and herbarium collections. *Journal of Tropical Ecology*, *36*(4), 159–173.

Ouédraogo, D.-Y., Beina, D., Picard, N., Mortier, F., Baya, F., & Gourlet-Fleury, S. (2011). Thinning after selective logging facilitates floristic composition recovery in a tropical rain forest of central africa. *Forest ecology and management*, *262*(12), 2176–2186.

Pan, Y., Birdsey, R. A., Phillips, O. L., & Jackson, R. B. (2013). The structure, distribution, and biomass of the world's forests. *Annual Review of Ecology, Evolution, and Systematics*, *44*, 593–622.

Pastick, N. J., Dahal, D., Wylie, B. K., Parajuli, S., Boyte, S. P., & Wu, Z. (2020). Characterizing land surface phenology and exotic annual grasses in dryland ecosystems using landsat and sentinel-2 data in harmony. *Remote Sensing*, *12*(4), 725.

Percival, D. B., Wang, M., & Overland, J. E. (2004). An introduction to wavelet analysis with applications to vegetation time series. *Community Ecology*, *5*(1), 19–30.

Philippon, N., Cornu, G., Monteil, L., Gond, V., Moron, V., Pergaud, J., Sèze, G., Bigot, S., Camberlin, P., Doumenge, C., et al. (2019). The light-deficient climates of western central african evergreen forests. *Environmental Research Letters*, *14*(3), 034007.

Philippon, N., De Lapparent, B., Gond, V., Sèze, G., Martiny, N., Camberlin, P., Cornu, G., Morel, B., Moron, V., Bigot, S., et al. (2016). Analysis of the diurnal cycles for a better understanding of the mean annual cycle of forests greenness in central africa. *Agricultural and Forest Meteorology*, *223*, 81–94.

Ranghetti, L., Boschetti, M., Nutini, F., & Busetto, L. (2020). sen2r": An r toolbox for automatically downloading and preprocessing sentinel-2 satellite data. *Computers & Geosciences*, *139*, 104473.

Ratnam, J., Bond, W. J., Fensham, R. J., Hoffmann, W. A., Archibald, S., Lehmann, C. E., Anderson, M. T., Higgins, S. I., & Sankaran, M. (2011). When is a 'forest'a savanna, and why does it matter? *Global Ecology and Biogeography*, *20*(5), 653–660.

Reich, P. B., & Borchert, R. (1984). Water stress and tree phenology in a tropical dry forest in the lowlands of costa rica. *The Journal of Ecology*, 61–74.

Réjou-Méchain, M., Mortier, F., Bastin, J.-F., Cornu, G., Barbier, N., Bayol, N., Bénédet, F., Bry, X., Dauby, G., Deblauwe, V., et al. (2021). Unveiling african rainforest composition and vulnerability to global change. *Nature*, *593*(7857), 90–94.

Richardson, A. D., Braswell, B. H., Hollinger, D. Y., Jenkins, J. P., & Ollinger, S. V. (2009). Near-surface remote sensing of spatial and temporal variation in canopy phenology. *Ecological Applications*, *19*(6), 1417–1428.

Roberts, D. A., Nelson, B. W., Adams, J. B., & Palmer, F. (1998). Spectral changes with leaf aging in amazon caatinga. *Trees*, *12*(6), 315–325.

Robinson, P. J., & Henderson-Sellers, A. (1991). *Contemporary climatology*. Routledge.

Rouse, J., Haas, R. H., Schell, J. A., Deering, D. W., et al. (1974). Monitoring vegetation systems in the great plains with erts. *NASA special publication*, *351*(1974), 309.

Ryan, C. M., Williams, M., Grace, J., Woollen, E., & Lehmann, C. E. (2017). Pre-rain green-up is ubiquitous across southern tropical africa: Implications for temporal niche separation and model representation. *New Phytologist*, *213*(2), 625–633.

Sakai, S. (2001). Phenological diversity in tropical forests. *Population Ecology*, *43*(1), 77–86.

Santiago, L. S., Bonal, D., De Guzman, M. E., & Ávila-Lovera, E. (2016). Drought survival strategies of tropical trees. *Tropical tree physiology* (pp. 243–258). Springer.

Sarmiento, G., & Monasterio, M. (1983). Life forms and phenology. *Ecosystems of the World*, *13*, 79–108.

Siebert, A. (2014). Hydroclimate extremes in africa: Variability, observations and modeled projections. *Geography Compass*, *8*(6), 351–367.

Silva, F. B., Shimabukuro, Y. E., Aragão, L. E., Anderson, L. O., Pereira, G., Cardozo, F., & Arai, E. (2013). Large-scale heterogeneity of amazonian phenology revealed from 26-year long avhrr/ndvi time-series. *Environmental Research Letters*, *8*(2), 024011.

Sims, D. A., & Gamon, J. A. (2002). Relationships between leaf pigment content and spectral reflectance across a wide range of species, leaf structures and developmental stages. *Remote sensing of environment*, *81*(2-3), 337–354.

Stendardi, L., Karlsen, S. R., Niedrist, G., Gerdol, R., Zebisch, M., Rossi, M., & Notarnicola, C. (2019). Exploiting time series of sentinel-1 and sentinel-2 imagery to detect meadow phenology in mountain regions. *Remote Sensing*, *11*(5), 542.

Stöckli, R., & Vidale, P. L. (2004). European plant phenology and climate as seen in a 20-year avhrr land-surface parameter dataset. *International Journal of Remote Sensing*, *25*(17), 3303–3330.

Sudmanns, M., Tiede, D., Augustin, H., & Lang, S. (2020). Assessing global sentinel-2 coverage dynamics and data availability for operational earth observation (eo) applications using the eo-compass. *International Journal of Digital Earth*, *13*(7), 768–784.

Suepa, T., Qi, J., Lawawirojwong, S., & Messina, J. P. (2016). Understanding spatio-temporal variation of vegetation phenology and rainfall seasonality in the monsoon southeast asia. *Environmental research*, *147*, 621–629.

Tutin, C. E., & Fernandez, M. (1993). Relationships between minimum temperature and fruit production in some tropical forest trees in gabon. *Journal of Tropical Ecology*, 241–248.

Van Schaik, C. P., Terborgh, J. W., & Wright, S. J. (1993). The phenology of tropical forests: Adaptive significance and consequences for primary consumers. *Annual Review of ecology and Systematics*, *24*(1), 353–377.

Veloso, A., Mermoz, S., Bouvet, A., Le Toan, T., Planells, M., Dejoux, J.-F., & Ceschia, E. (2017). Understanding the temporal behavior of crops using sentinel-1 and sentinel-2-like data for agricultural applications. *Remote sensing of environment*, *199*, 415–426.

Verbeeck, H., Boeckx, P., & Steppe, K. (2011). Tropical forests: Include congo basin. *Nature*, *479*(7372), 179–179.

Vrieling, A., Meroni, M., Darvishzadeh, R., Skidmore, A. K., Wang, T., Zurita-Milla, R., Oosterbeek, K., O'Connor, B., & Paganini, M. (2018). Vegetation phenology from sentinel-2 and field cameras for a dutch barrier island. *Remote sensing of environment*, *215*, 517–529.

White, M. A., de Beurs, K. M., Didan, K., Inouye, D. W., Richardson, A. D., Jensen, O. P., O'KEEFE, J., Zhang, G., Nemani, R. R., van Leeuwen, W. J., et al. (2009). Intercomparison, interpretation, and assessment of spring phenology in north america estimated from remote sensing for 1982–2006. *Global Change Biology*, *15*(10), 2335–2359.

Wingate, L., Ogée, J., Cremonese, E., Filippa, G., Mizunuma, T., Migliavacca, M., Moisy, C., Wilkinson, M., Moureaux, C., Wohlfahrt, G., et al. (2015). Interpreting canopy development and physiology using a european phenology camera network at flux sites. *Biogeosciences*, *12*(20), 5995–6015.

WRB, IUSS Working group. (2014). *World reference base for soil resources 2014. international soil classification system for naming soils and creating legends for soil maps*. FAO. Rome.

Wright, S. J., & Calderón, O. (2006). Seasonal, el niño and longer term changes in flower and seed production in a moist tropical forest. *Ecology letters*, *9*(1), 35–44.

Wright, S. J., & Van Schaik, C. P. (1994). Light and the phenology of tropical trees. *The American Naturalist*, *143*(1), 192–199.

Xiao, X., Hagen, S., Zhang, Q., Keller, M., & Moore III, B. (2006). Detecting leaf phenology of seasonally moist tropical forests in south america with multi-temporal modis images. *Remote Sensing of Environment*, *103*(4), 465–473.

Xue, J., & Su, B. (2017). Significant remote sensing vegetation indices: A review of developments and applications. *Journal of sensors*, *2017*.

Yan, Y. Y. (2005). Intertropical convergence zone (itcz). In J. E. Oliver (Ed.), *Encyclopedia of world climatology* (pp. 429–432). Springer Netherlands. https://doi.org/10.1007/1-4020-3266-8_110

Yoshioka, H., Miura, T., & Obata, K. (2012). Derivation of relationships between spectral vegetation indices from multiple sensors based on vegetation isolines. *Remote Sensing*, *4*(3), 583–597.

Yu, L., Liu, T., Bu, K., Yan, F., Yang, J., Chang, L., & Zhang, S. (2017). Monitoring the long term vegetation phenology change in northeast china from 1982 to 2015. *Scientific reports*, *7*(1), 1–9.

Zeng, L., Wardlow, B. D., Xiang, D., Hu, S., & Li, D. (2020). A review of vegetation phenological metrics extraction using time-series, multispectral satellite data. *Remote Sensing of Environment*, *237*, 111511.

Zhang, X., Friedl, M. A., Schaaf, C. B., Strahler, A. H., & Liu, Z. (2005). Monitoring the response of vegetation phenology to precipitation in africa by coupling modis and trmm instruments. *Journal of Geophysical Research: Atmospheres*, *110*(D12).

Zhu, Y., Liu, K., Liu, L., Myint, S. W., Wang, S., Liu, H., & He, Z. (2017). Exploring the potential of worldview-2 red-edge band-based vegetation indices for estimation of mangrove leaf area index with machine learning algorithms. *Remote Sensing*, *9*(10), 1060.

Chapter 6

Appendices

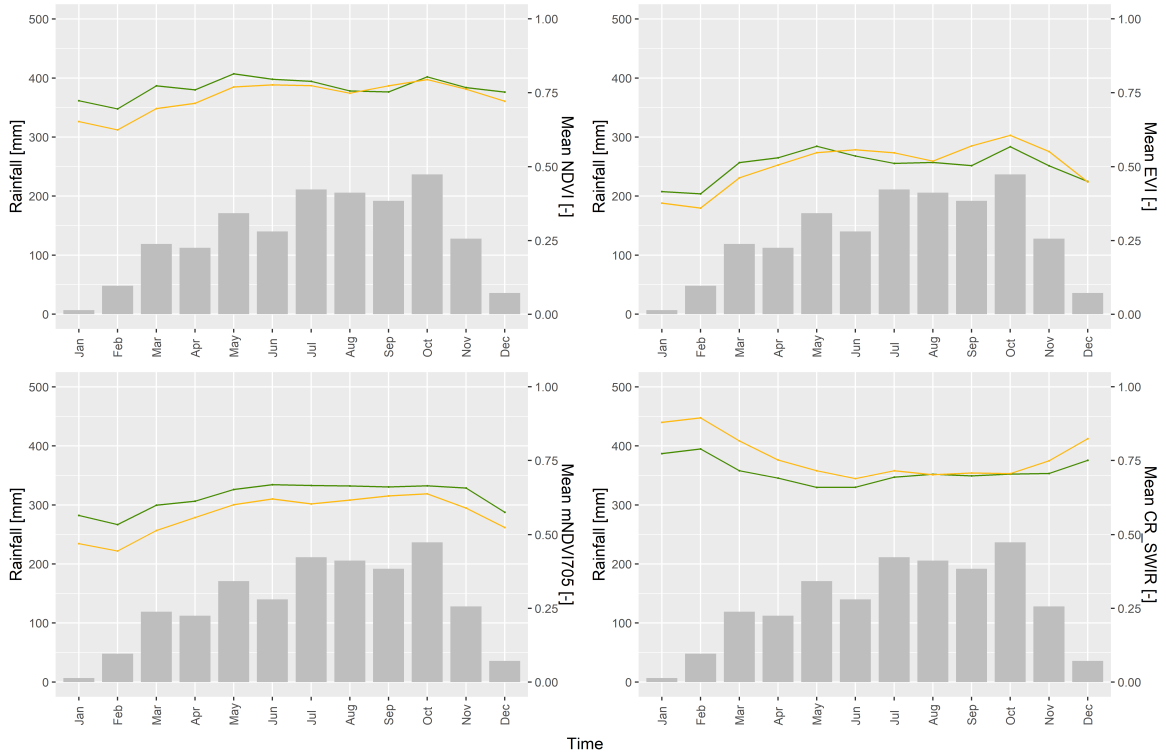

Figure 6.1: Synthetic year of NDVI, EVI, mNDVI705 and CR_SWIR for each Land Cover Class. Each index value is monthly averaged over the study site (MBaïki) and over the study period (2015-2020). The bars are the monthly accumulated rainfall averaged yearly. In dark green, the forest pixels. In yellow, non-forested pixels, including mostly savannas and then, fallows and crops.

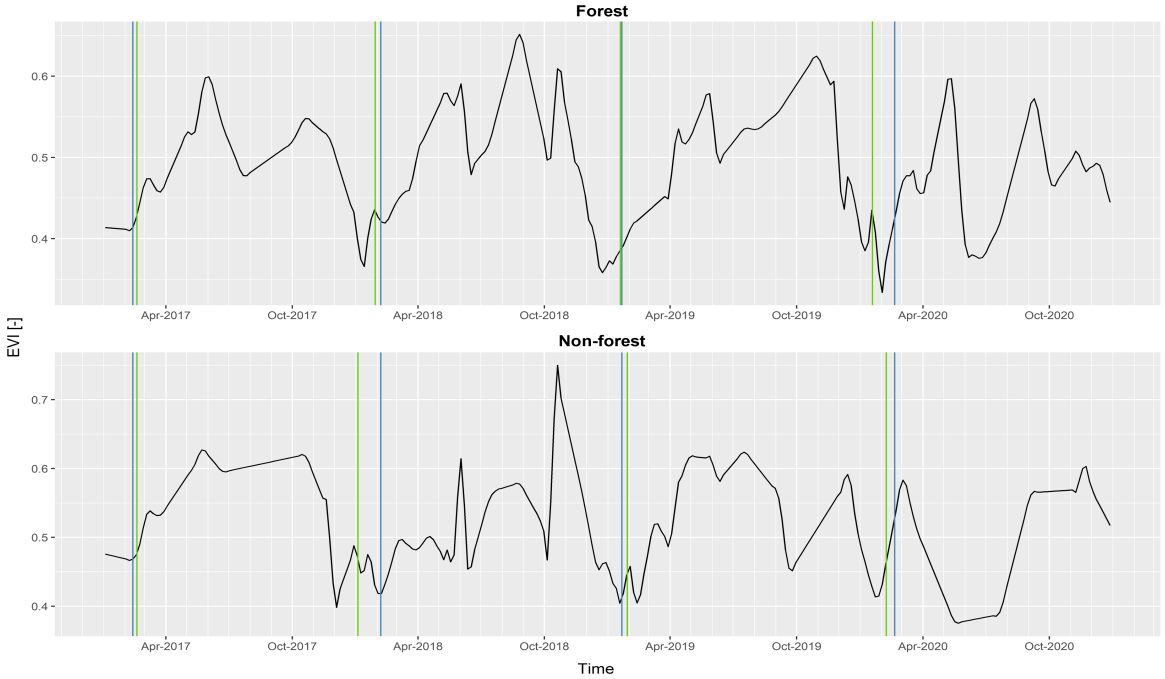

Figure 6.2: Savitsky-Golay smoothed EVI mean time series for one randomly chosen pixel of each land cover class. The vertical green and blue lines represent respectively the Start Of the Season (SOS) and the Start Of Rain (SOR) for 2017-2019. Site: MBaïki.

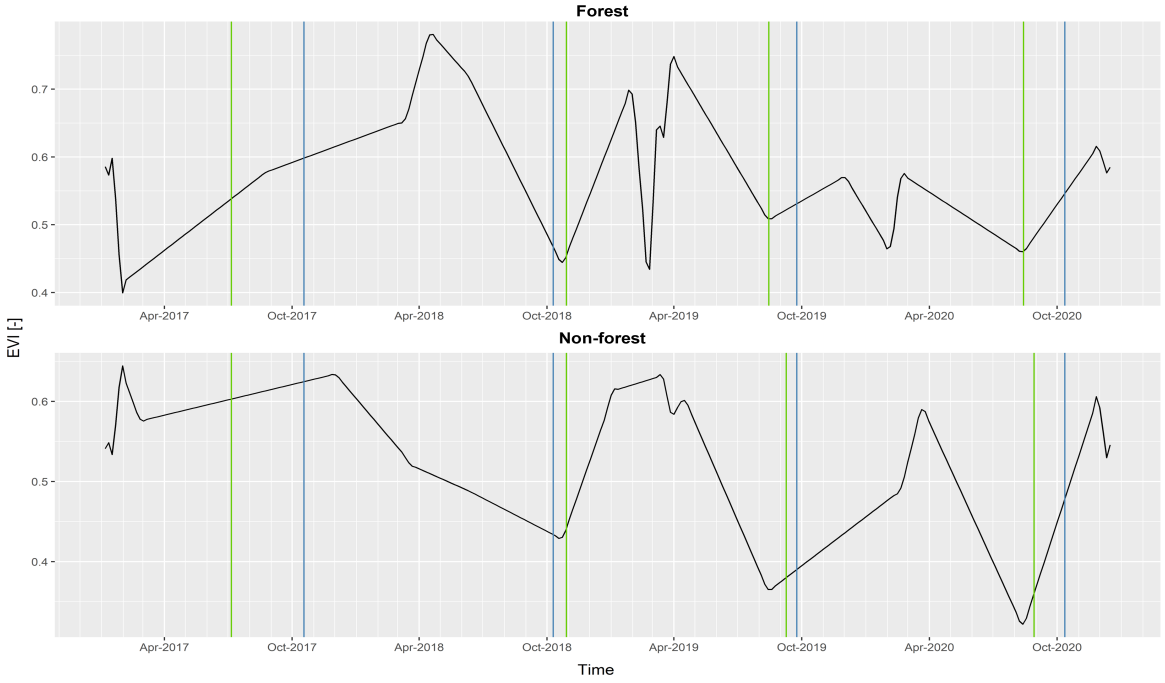

Figure 6.3: Savitsky-Golay smoothed EVI mean time series for one randomly chosen pixel of each land cover class. The vertical green and blue lines represent respectively the Start Of the Season (SOS) and the Start Of Rain (SOR) for 2017-2019. Site: Luki.

Table 6.1: Time required to perform each of the main computational steps. Those approximate numbers are obtained with a basic computer equipped with a i5 processor and a 8 Go RAM.* Considering an Internet speed of 5MB/s and an average file size of 700MB.

Step	**Time (hours)**
Download and unzip	0.038*/image
Sen2cor algorithm	0.5 /image (sen2cor 2.8), 0.7/image (sen2cor 2.5.5)
Crop, resample and cloud mask	3
Compute spectral indices	2
Spatial aggregation: time series	4
SOS and SOR retrieval	5.5
Ground validation	0.5
BioDivMap R	0.2
Wavelets	0.1

Table 6.2: Space disk required for the main datasets considering one study site (Mbaïki in this case).

Description	**Size [GB/image]**	**Total [GB]**
Level-1C	0.7	184
Level-2A	1	264
Crop and stack raster	0.1	66.2
Index raster	0.02	
GPM data	world	61.2
Total		575.4